Spatial Characterisation of a Laser-Produced X-ray Source

Diploma paper
by
Arne Nykänen

Lund Reports on Atomic Physics, LRAP-210
Lund, February 1997

Abstract

Hard X-rays have been generated by focusing 110 fs laser pulses to intensities of about 10^{17} W/cm^2 on a solid target. The source must be spatially characterised in order to investigate the possibilities of using this kind of X-ray source for magnification radiography. The size and the intensity distribution of the source were measured. Four measurement methods were used and evaluated: measurements with a pinhole, a slit, and a star-test pattern, and measurement of the edge-spread function of a thread. All methods showed good agreement. Most measurements were done with pinhole, since this method gives two-dimensional information on the intensity distribution of the source. This distribution was found to be approximately circular symmetric, with an intensity profile approximately fitted by a Lorentzian curve. Source sizes down to a diameter of about 30 µm were measured (FWHM). The influence of different parameters on the source size was investigated. Parameters changed were: the laser energy, the size of the laser focus, filtration of the X-ray radiation, laser prepulses and surface roughness of the target. No significant changes could be seen, except for a correlation between the laser focus size and the X-ray source size.

1. Introduction

The most common way to produce X-ray radiation today is to accelerate electrons in an electric field and let them hit a target of some high atomic number material, usually tungsten[1,2]. This is done in conventional X-ray tubes used for medical imaging. Another way is to use synchrotron radiation[3,4]. For therapy also other photon sources such as gamma-emitting radionuclides are used.

One way to produce X-rays, not yet developed for medical imaging, is to focus high-power laser pulses on a solid target[5]. This will create a plasma. If the plasma temperature is high enough, fast electrons will be generated and slowed down in the target material. This will give rise to X-rays by emission of Bremsstrahlung and characteristic X-rays. The terawatt laser system at the Lund High-Power Laser Facility has been used[6]. This system can deliver pulses of 110 fs duration with an energy of about 150 mJ per pulse. The peak power is 10^{12} W, the wave-length 794 nm and the repetition rate is 10 Hz. The focused intensity on the target surface is of the order of 10^{17} W/cm^2. With these high laser intensities hard X-rays will be emitted. The X-ray spectrum will extend from around 10 keV (softer radiation will be filtered away by the exit window of the experimental chamber), with decreasing intensity up to the MeV-region, with peaks at the characteristic energies of the target material.

The characteristics of this X-ray source are small spatial dimensions[7], extremely short pulses with a high peak flux[8], and a relatively large fraction of characteristic X-rays[5]. The short pulses can be used for time-gated imaging[9,10,11], a technique for scatter-reduced imaging. The pulse lengths in the picosecond range also makes it possible to record images of extremely fast events. This kind of fast events do not occur in the human body, but can be interesting for technical imaging and basic research. The large fraction of characteristic X-rays make these sources appropriate for differential imaging[12]. This is done by using a contrast agent and two different targets, one with the K-emission lines just below the K-absorption edge of the contrast agent and one with the emission lines just above. Two pictures are taken, one with each of the targets. By dividing or subtracting these, parts of the object containing the contrast agent will stand out more clearly in the resulting picture. This can be compared with standard techniques for subtraction angiography[2]. The small spatial dimensions of laser-produced-plasma (LPP) sources make them suitable for magnification radiography, both for imaging of small structures and for reduction of the amount of scattered radiation[13,19,23]. The high magnification can be used for medical purposes, e.g. observation of microcalcifications in women breast, which can be a pre-state to breast cancer[23,24,25], and to look at the microstructure of bones[19].

In order to evaluate the magnification imaging potential of the LPP X-ray source the source size and the intensity distribution of the source have been measured. For the actual X-ray source only one measurement has been done previously. This was instrumentation limited, but showed that the diameter of the source was less than 60 μm[8]. The aim of the study presented in this work was to measure and evaluate the size and intensity distribution of the source, and to estimate the smallest resolvable structure size. Different techniques were evaluated and applied to measurements. The techniques used were pinhole, slit, edge and star-pattern imaging. The pinhole technique was found to be the most convenient technique to achieve information on intensity distribution and source size in most cases. Problems common to all the

techniques are the poor contrast due to penetration of high-energy photons. Additionally, the small spatial dimensions of the source demands the ability to measure high spatial frequencies. Source sizes down to a diameter of around 30 µm (FWHM) have been measured, but very large fluctuations between different measurements were seen (from 30 µm up to 100 µm). The intensity distribution of the source showed out to be approximately Lorentzian. The influence of different parameters such as laser energy, laser pre-pulses and filtration of the X-ray beam on the source size was investigated, but no significant changes were seen. However, a correlation between laser focus size and the X-ray source size was found. The large fluctuations in the source size though make these evaluations difficult.

Higher magnification is expected to lead to a higher dose to the patient. There have been many studies on the dose to the patient when magnifying techniques with conventional X-ray tubes are used[13,19,23,24,25]. These studies shows that the increase in dose is not very large, and can be motivated by gained security in diagnosis in many cases. Better sources would probably develop these methods further.

The low repetition rate of currently available table-top terawatt lasers results in too long exposure times for medical imaging in most cases, due to the low average X-ray flux rates. However, it can be used for magnification imaging of objects that can be fixed for longer exposure times. The evolution of lasers today goes towards higher repetition rates and higher peak powers. This can make the laser produced X-ray sources competitive with conventional X-ray tubes in some applications.

2. Theory

2.1 Laser produced plasmas

Plasma is considered as the fourth state of matter, a state where matter is either partially or completely ionised. In other words, the plasma consists of ions, electrons, atoms and molecules. Different parameters can be used to characterise a plasma, e.g. the electron and ion temperatures, a measure of the velocity distributions of electrons and ions, respectively, and charge densities. Short interaction range between different particles in the plasma makes collective effects most important. The electron mobility in a plasma is very high, while the mobility of ions is low. Differences in the electric potential in a plasma are therefore equalised by movement of electrons. This makes the plasma essentially neutral. Collective effects that can occur are, for example, plasma oscillations. This is a collective oscillating motion of electrons relative to the positive ions. If electrons are collectively moved from their equilibrium position the plasma will be polarised. The electrons will be attracted to the equilibrium position and collective oscillation of electrons will occur. The angular frequency of the oscillation, ω_p, called the plasma frequency, is given by the following expression:

$$\omega_p = \left(\frac{n_e e^2}{m_e \varepsilon_0} \right)^{1/2} = 56.4 n_e^{1/2}, \qquad (1)$$

where n_e is the electron number density in m^{-3}, ε_0 is the permittivity constant, m_e is the electron rest mass and e is the unit charge. There is a corresponding frequency for ionic oscillations, obtained by replacing the electron mass in the equation above by the ionic mass. In the presence of a magnetic field the electrons and ions can also spiral around the field lines with characteristic frequencies, called cyclotron frequencies. The response of the plasma to external oscillating fields is depending on all these natural frequencies. If the frequency of an incoming wave matches one of the characteristic frequencies, or some combination of them, resonance interaction can occur, leading to enhanced energy transfer from the wave to the plasma. Considering only the plasma frequency, the dispersion relationship determining the propagation of electromagnetic radiation is given by:

$$\omega^2 = \omega_p^2 + c^2 k^2, \qquad (2)$$

where ω is the angular frequency, and $k=2\pi/\lambda$ is the wave number. If $\omega_p<\omega$, k is real, and the elector-magnetic radiation propagates. If $\omega_p>\omega$, k is imaginary and the plasma becomes opaque. In a laser-produced plasma an electron density gradient exists, consequently varying the plasma frequency ω_p. Reflection occurs at the density corresponding to $\omega_p=\omega$. This is called the critical density, n_c, and is given by:

$$n_c = \frac{\varepsilon_0 m_e \omega^2}{e^2} = 3.14 \cdot 10^{-4} \omega^2 \qquad (3)$$

Dense plasmas will reflect at optical frequencies, and this will be an important effect for laser-produced plasmas. The group velocity of the electromagnetic wave is given by:

$$v_g = \frac{d\omega}{dk} = c\sqrt{1 - \omega_p^2/\omega^2} \qquad (4)$$

This is a measure of the speed at which the energy in the wave is transported. In the region near n_c, the group velocity is very low, giving a high probability for energy to be absorbed by the plasma.

When a metal surface is irradiated with laser radiation the radiation only penetrates to a depth of typically a fraction of a wavelength. This results in an interaction with the conducting electrons, leading to heating, evaporation and ionisation. A thin sheet of plasma close to the target surface is produced. This plasma, with a relatively low plasma temperature, can be seen as an initiation stage for other energy absorption processes. For low-temperature plasmas, the dominating light absorption process is inverse Bremsstrahlung. A hot plasma becomes essentially collisionless, and therefore the heating due to inverse Bremsstrahlung decreases rapidly when the plasma temperature increases. This effect becomes important when laser intensities above 10^{17} W/m^2 is used. However, experimental data show increasing absorption with increasing intensity in this region[14]. This increase can be explained by collective absorption due to excitation of plasma waves.

There are two main ways of energy transfer from laser light to plasma waves: resonant absorption and non-linear parametric absorption. Resonant absorption occurs when an electromagnetic wave is incident on a plasma at a nonzero angle of incidence, θ. The electric polarisation vector, **E**, is lying in the plane of incidence. The electromagnetic wave will be deflected in the plasma according to Figure 1.

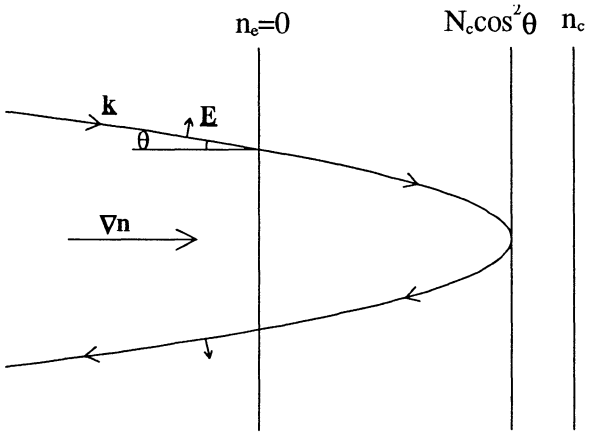

Figure 1 (taken from ref.14), Deflection of electromagnetic wave incident on plasma.

If the turning point, $n_e=n_c\cos^2\theta$, is close enough to the critical density zone, $n_e=n_c$, the electric field can tunnel into that zone and drive resonant plasma oscillations there. This effect is depending on the polarisation of the incoming wave. If **E** is perpendicular both to **k** and **∇n**, there will never be a component of **E** parallel to **∇n** and the incoming wave will not drive the resonance mechanism. The resonance absorption will have a peak at some value of θ. At small angles of incidence the **E**-component of the electromagnetic wave parallel to the density gradient, **∇n**, is small, and for large angles the wave will be reflected far away from the critical region so that the wave will not be

efficiently coupled. The peak of the resonance absorption will therefore be at some intermediate value of θ.

In the case of non-linear parametric absorption the energy is transferred from the incident wave with frequency ω_0, to two plasma oscillation frequencies, ω_1 and ω_2. The condition $\omega_0=\omega_1+\omega_2$ must be fulfilled. Resonant coupling will occur when the frequency of the incident electromagnetic wave equals a beat frequency of the plasma oscillations.[14,15,16,17]

The X-rays emitted from a laser-produced plasma are mainly produced as Bremsstrahlung from fast electrons slowing down in the plasma and in the surrounding target material. The laser pulses used in the experimental set-up have a duration of about 110 fs. The energy of these pulses can be deposited in the target before any considerable expansion will occur. This will give rise to a very high density gradient, which will allow for a fast expansion and a high heat conduction into the solid. Consequently the plasma will be cooled down fast, and the X-ray emission will be terminated within a few ps.[18]

2.2 Magnification radiography

2.2.1 Technical concepts

Magnification radiography is used mainly for two reasons: to increase the resolution of the imaging system and to suppress the influence of scattered radiation on the image (called the air-gap technique). This technique is most common in mammography[23,24,25], but can also be used on other parts of the body, mainly to see small structures in bones[19,20].

To describe the properties of an imaging system, the point spread function (PSF) (or in one dimensional cases, the line spread function (LSF)), and the modulation transfer function (MTF), are used[21]. The PSF is defined as the two-dimensional distribution function of the picture of an infinitesimally small hole. The LSF is the one-dimensional distribution function of the picture of an infinitesimally narrow slit. Two conventional ways of defining the spatial source size exist. One is to take the Full Width at Half Maximum (FWHM) of the source intensity distribution. Another way is to use the Width of a Rectangular Distribution with Equal Area and Maximum value (WRDEAM). The MTF describes the ratio between the contrast in the image and the contrast in the imaged object as a function of spatial frequency. It can be calculated as the Fourier transform of the LSF (1-dim.) or the PSF (2-dim.). The MTF is a measure of how an imaging system can resolve small details. If the MTF of each part of an imaging system (i.e. film/detector, intensifying screen, focal spot, object motion) is known the total MTF of the system is the product of each part. This is a good tool while optimising the magnification of a system, since a higher magnification leads to lower MTF of the focal spot, but a higher MTF of the detector. When measuring the MTF, often a binary object set with lines and spaces are used. Since the MTF is defined for sinusoidal spatial frequencies the use of binary objects will only give an approximation to the MTF. The measured function is called the contrast transfer function (CTF), and is often a good approximation[22].

2.2.2 Medical applications

Today the most common application of magnification radiography is in mammography. It is desirable to detect small calcifications in women breast, since they can be a pre-state to cancer. These calcifications can be as small as 0.1 mm, and to be able to do safe diagnosis a high resolution is needed. A conventional way of solving this is by using an X-ray tube with a focal spot size of ~0.1 mm, a magnification of ~2 and a film with intensifying screens[23]. Often the detector, for example an intensifying screen, is the limiting factor of the system. Due to the small loadability (i.e. low X-ray flux rate) of the microfocus X-ray tube, sensitive detectors must be used. These often have poor resolution. With a stronger source a less sensitive detector with higher resolution can be used, but the lower sensitivity leads to a higher dose to the patient. A higher magnification also gives a higher resolution to the system, demanding a smaller source, but allowing a detector with lower resolution and higher sensitivity. The most suitable configuration has to be determined for every kind of examination.

The use of high magnification radiography (up to 10 x) for examination of small structures in bone is described by Buckland-Wright and Bradshaw[19]. They have tried even higher magnifications, but patient movement then became a problem. With a source with higher X-ray flux rate this problem would have been reduced. In their clinical studies they have shown that diagnosis of arthritic and metabolic disorders can be done by magnification imaging of bones and joints.

The patient dose in magnification radiography compared to contact radiography have been investigated in a number of articles concerning mammography[23,24,25] and radiography of bones and joints[19]. The increase in dose for magnifying techniques has been found to be small. Often a higher magnification allows more sensitive detectors with lower resolution, reducing the increase in dose introduced by the higher magnification. The increase in dose must be motivated by the increased safety in diagnosis, and the system must be optimised with respect to resolution and patient dose. Here a small source with high X-ray flux rate is desired.

The biological effect of the extremely short and intense X-ray pulses coming from a LPP has been studied by C. Tillman et al.[26]. The survival of cells irradiated with extremely high dose-rates (up to 10^9 Gy/s) did not differ much from cells irradiated with much lower dose rates from conventional X-ray tubes (< 1 Gy/s).

3. Experimental set-up

3.1 The terawatt laser system

The laser system used in the experiments was the terawatt laser of the Lund High-Power Laser Facility[6]. In high-power lasers the damage thresholds of optical materials put constraints on the maximum laser intensity. One way to avoid optical damage is to increase the diameter of the laser beam. This demands large-scale optics that are very expensive. Instead, the terawatt laser in Lund uses the chirped-pulse amplification technique. The basic idea of this technique is to stretch an initially short pulse in time before amplification, consequently reducing the peak power in the amplifier. After amplification, the pulse is recompressed in time to achieve extremely high peak powers (Figure 2).

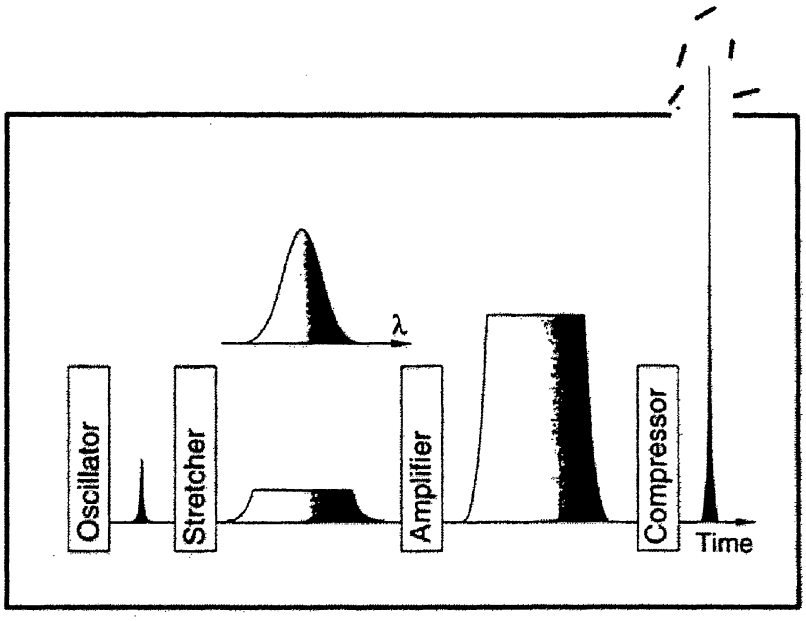

Figure 2 (taken from ref. 6)**:** The principle of chirped-pulse amplification.

A schematic diagram of the laser system is shown in Figure 3, and the optical layout is shown in Figure 4. The system uses an Ar^+-laser-pumped mode-locked Ti:Sapphire oscillator generating 110 fs laser pulses with a repetition rate of 76 MHz and an average power of 0.76 W (10 nJ/pulse, 100 kW peak power). The short pulse width corresponds to a large bandwidth. This is needed since the principle of the stretcher and the compressor is that light of different wavelengths will have different pathlengths. By arranging a pair of gratings as in Figure 5, different spectral components experience different temporal delay, and the pulse will be stretched or compressed. The stretched pulses are passed through two Ti:Sapphire amplifiers, which are pumped with frequency-doubled Nd:YAG laser light. After this the pulse is compressed to 110 fs, yielding powers up to 1 TW in the region 760-840 nm. The maximum output is achieved at 794 nm, which was the wavelength used for the experiments in this study. The repetition rate of the system is 10 Hz.

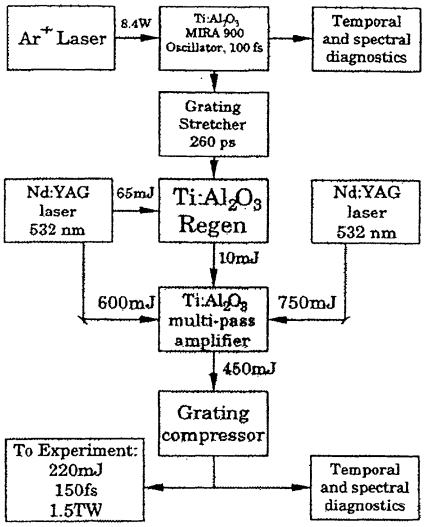

Figure 3 (taken from ref. 6): A schematic diagram over the terawatt laser-system in Lund.

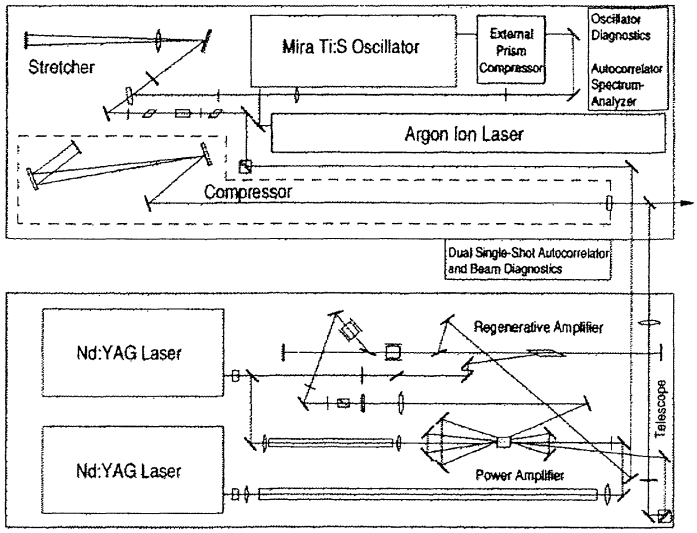

Figure 4 (taken from ref. 6): Optical layout for the terawatt laser-system in Lund.

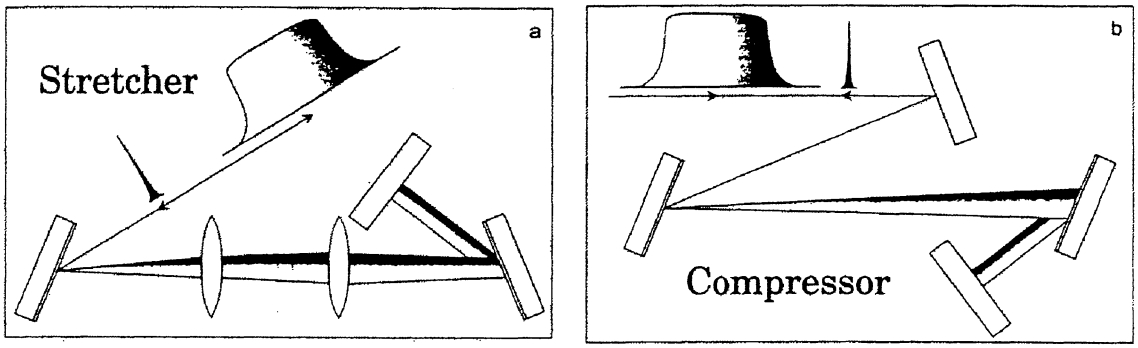

Figure 5 (taken from ref. 6): Principles of the laser-pulse stretcher and compressor.

3.2 The experimental chamber

To produce incoherent hard X-ray radiation a laser intensity of approximately 10^{17} W/cm^2 was used. To be able to focus the beam to such high intensities without causing electrical breakdown, the experiments must be done in vacuum. The experimental chamber is described in detail by C. Tillman [5]. The chamber is made of a 30 mm thick aluminium frame with 20 mm thick aluminium bottom and top lids. Two windows give access to the chamber: the laser pulse entrance window, made of 10 mm thick BK7 glass with an optical surface roughness of less than $\lambda/12$ at 800 nm and the X-ray outlet window, made of 0.2 mm polyethylene film. The transmission of photons with an energy above 10 keV in such a film is more than 95 %. For radiation protection the whole chamber is covered by 5 cm thick lead bricks.

To focus the laser beam on the target a parabolic mirror is used. Lenses cannot be used because the short focal length requires a thick lens. This will cause prolongation and self-phase modulation of the laser pulses. The effective focal length of the mirror is 50 mm, the diameter 50 mm, and it is chromium-gold coated with a surface roughness

of λ/5 at 800 nm. To protect the mirror from sputtered particles from the target a glass plate is placed in the laser beam, between the mirror and the target. The targets used are made of some metal with high atomic number, e.g. tantalum or tungsten. Experiments with other materials, such as copper and molybdenum, have also been done. Foils of the target material are fixed on steel discs. These discs are mounted in a rotating holder, resting on three points, two of which can be adjusted to reduce wobbling of the target. The target holder is motorised, so it can be moved along the rotational axis to be able to get the disc surface to focus. It can also be moved perpendicular to the rotational axis to change the track without opening the chamber. The target is actively stabilised by measuring the position with a mechanical micrometer with electrical read-out and by regulating the position with a piezo-electric translator on the target holder. The stabilisation is controlled by a PC.

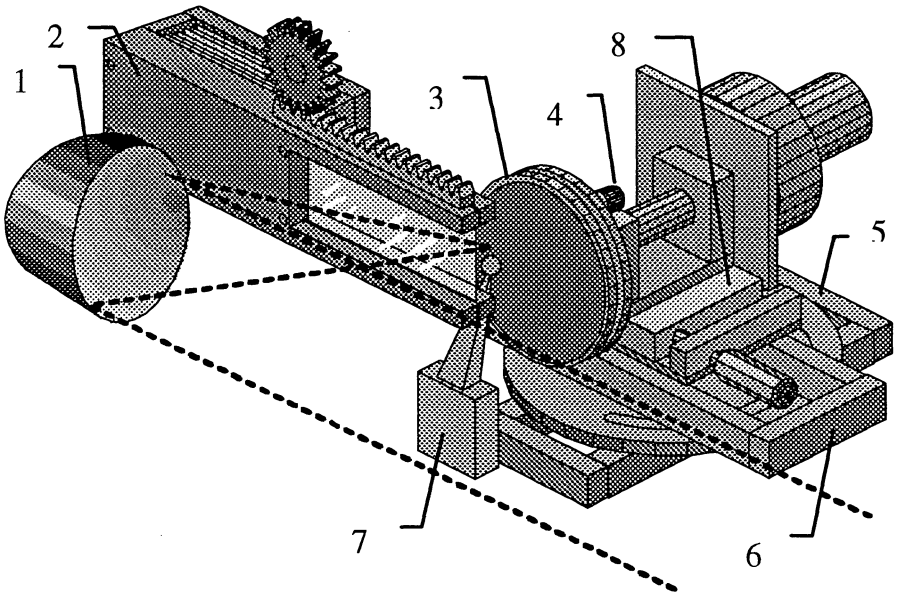

Figure 6: The set-up in the chamber: The mirror (1) is protected from sputter by a thin glass-plate in a glass-feeder (2). The laser beam is focused on the target (3) by the mirror. The target can be adjusted to minimise wobbling by two adjustment screws on the holder (4), and can be moved by the translators (5 and 6). The target is also actively stabilised by measuring its position with a mechanical micro-meter (7) and by regulating the position with a piezo-electric translator (8).

3.3 Imaging systems

Two different systems have been used for imaging, digital image plates and a CCD-system:

Image plates[27,28] are the most frequently used digital imaging system for radiography. These plates consist of a crystal layer of europium-doped bariumfluorohalide on a plastic substrate. The crystal contains luminescence centres where electrons are trapped when it is irradiated with X-ray photons. These electrons are released when the crystal is illuminated with light from an HeNe-laser (633 nm), leading to emission of luminescence light at 400 nm. The emitted light is detected with a photomultiplier

tube as the plate is scanned with the laser beam. These plates have a number of advantages compared to photographic film.

- They are much more sensitive than film,
- have a dynamic range of 10^4-10^5, compared to films with a dynamic range of 10^2,
- have a linear dose response, and
- can be reused.

The image plates (Fuji BAS2000, Fuji Photo Film Co., Ltd, Japan.) were used in standard film cassettes, usually used at hospitals. A spatial resolution of 0.2 mm was used for practical reasons.

A system consisting of a scintillating fibre-optic plate (LKH-6)[29], an image intensifier and a CCD camera have been used, to get better spatial resolution and immediate read-out. The CCD array itself can not be used, since it is only sensitive to soft X-ray radiation (up to 20 keV). Instead, it has been used to measure the light emitted from the scintillator, intensified by the image intensifier. Two different coupling optics between the image intensifier and the CCD array have been used, giving 0.053 mm and 0.022 mm resolution, respectively. The optics with better resolution also gave rise to more aberrations, and had an inhomogeneous throughput, that varied much from the centre and out to the periphery. The average throughput was however much better than for the other lens, allowing shorter exposure times. To compensate for the position dependent throughput and spatial variations in intensifier gain, an exposure without any object was taken, and used for normalisation.[30]

4. Measurement methods

Since hard X-rays are difficult to focus, the only way to get information on the intensity distribution of an X-ray source is to make an image of some kind of shadowing object with it. The size and the distribution can be determined from this image. The most direct way of measuring the size and intensity distribution is to use a small hole. This will give a picture of the X-ray source. If a narrow slit is used instead, this will result in a one-dimensional distribution. Other possible methods are to use an edge or some kind of repeating pattern, but this will demand deconvolution of the picture to give the intensity distribution of the source. This kind of deconvolution is often difficult to do in practice since the noise in the picture will give strong contributions to the results and often completely drown the desired information. The advantage of using repeating patterns is that they give a direct measure of the maximum resolving power of the system. Hard X-rays demand thick objects to give good image contrast. This is a problem when small source sizes are to be measured. The small source size demands an object containing high spatial frequencies, i.e. small gaps/holes, patterns with high spatial frequency and very sharp edges. It is difficult to produce this kind of thick objects with high spatial frequencies, and it is important to align them well when using them.

4.1 Pinhole camera

To get good pictures of the source without complicated deconvolution a pinhole with a size much smaller than the source itself can be used. However, the small size of the hole, with its correspondingly low throughput, leads to long exposure times. SEM-apertures used in electron microscopy turned out to be convenient for pinhole imaging. These apertures are produced in platinum-iridium alloy (95%/5%) and they are 170 µm thick (se Figure 7). Therefore they have good absorption, resulting in good contrast, even at high photon energies. 5 µm and 10 µm holes have been used in this study. Since the 5 µm hole is 33 times thicker than wide it is very critical that it is correctly aligned. This was done by pointing a HeNe-laser at the focal point of the terawatt laser beam from approximately 3 m distance. Then the pinhole was inserted and centred in the HeNe-beam. Since the apertures were almost flat and polished on one side, the back reflection of the HeNe-beam could be used to adjust the angle of the pinhole. The pinhole was fixed in a holder with translators. It could also be tilted to adjust the angles. This facilitated the process of alignment.

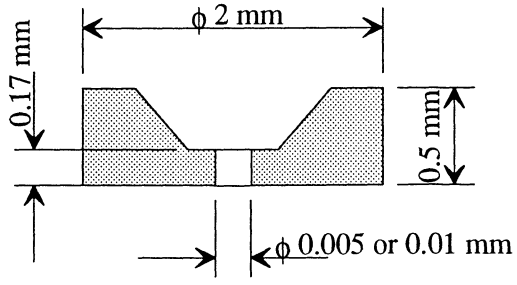

Figure 7: Cross section of the SEM-aperture made of platinum-iridium alloy (95%/5%), used as pinhole.

4.2 Slit

A problem with pinhole measurements is that the photon flux transmitted through the pinhole is low. This results in significant noise in the measured intensity profiles. To lower the noise a one-dimensional picture, using a slit can be taken. This makes it possible to integrate over one direction when taking the intensity distribution from the picture, resulting in lower noise levels. As in the case of pinholes this method demands a slit-width much smaller than the size of the source. In the present study a slit with platinum-iridium jaws and adjustable slit width, usually used for standard measurements on radiographic equipment was used. The slit was shaped according to the International Standard[31] (Figure 8). The V-shape of the jaws made the alignment quite uncritical. The slit used had a minimal slit width of 16 µm. The holder of the slit was rather big, and could not be placed close to the source. Therefore, the image plates had to be placed far from the slit to get a satisfying magnification, leading to long exposure times. The large slit width and the long exposure times made this slit inconvenient for this study, but some exposures were done for comparison between the different methods.

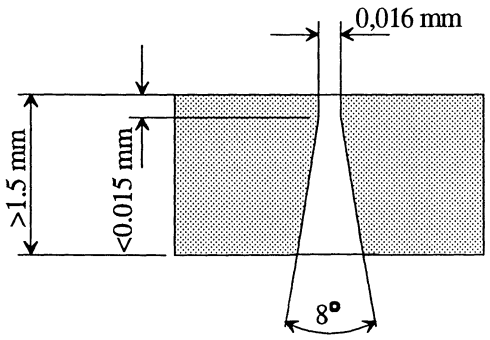

Figure 8: Slit, shaped according to the International Standard[31].

4.3 Measuring the edge-spread function

Instead of measuring the width of the point- or line-spread functions, the size of the source can be determined from the edge-spread function (ESF). Information on the source size and intensity distribution can be found in the penumbra region in the image of the edge. The ESF can be measured by having a plate of some attenuating material with a sharp edge, thick enough to attenuate most of the radiation. This kind of arrangement is difficult to align, but can be useful to get good contrast when investigating sources with higher X-ray energies[32]. In this study a thick (0.5 mm) platinum thread has been used. However, the thread is an inhomogeneous absorber, and the transmission varies at different positions (Figure 9). This affects the penumbra region, and must be taken into consideration.

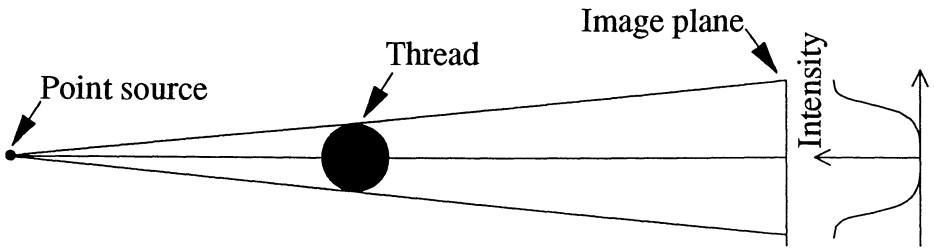

Figure 9: The intensity distribution of a thread irradiated with an X-ray point source. No sharp edge is achieved, due to a decreasing absorption pathlength at the edges of the thread.

In a first approximation the thread is considered to attenuate all photons, even in the periphery. This will overestimate the size of the source. This overestimation has been calculated and the measurements have been corrected (see 4.6.4). One benefit of using a thread compared to measurements with pinhole or slit is that no alignment is needed. The method allows for reproducible and easy measurements of the source size. However, the systematic errors can be quite large, and have to be thoroughly investigated and corrected for. Another benefit is that it is also possible to do measurements with different filtration in the same exposure by covering parts of the thread with different filters. All filters can be exposed at the same time. This ensures that the source size is the same in all measurements done in that single exposure. All measurements with thread were done on image plates. The low resolution of the plates (0.2 mm) required high magnification, resulting in long exposure times (~5 min).

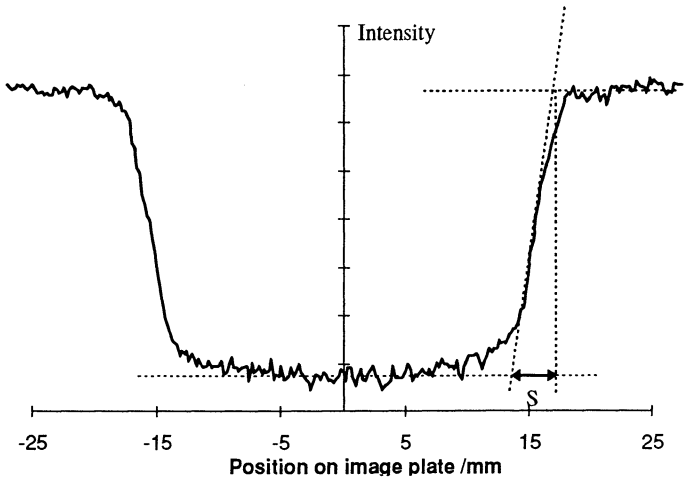

Figure 10: Intensity profile on image plate of a 0.5 mm Pt-thread at 60 times magnification. S divided by the magnification is equal to the WRDEAM.

Information on the intensity distribution and source size can be found in the penumbra region, as shown for a typical measurement in Figure 10. According to Maudsen[33], the distance S in the figure corresponds to the Width of Rectangular Distribution with Equal Area and Maximum value, WRDEAM. S is obtained by construction the tangent line at the point where the intensity curve has its maximum slope.

4.4 Star-test pattern

The use of a star-test pattern is a direct way of measuring the resolution of an imaging system. The pattern consists of a number of bars and spaces in a star shape (see Figure 11). When the pattern is imaged, the picture will be blurred when the pattern reaches a spatial frequency larger than the maximum resolution of the system. The size of the source can be estimated from this resolution, but it can not be absolutely determined, since the resolution depends on both the size and the intensity distribution of the source. A CTF-curve can be measured by scanning the picture of the pattern at a number of places and plot the contrast between the bars and the spaces as a function of spatial frequency. The CTF can be used as a good approximation to the MTF[22].

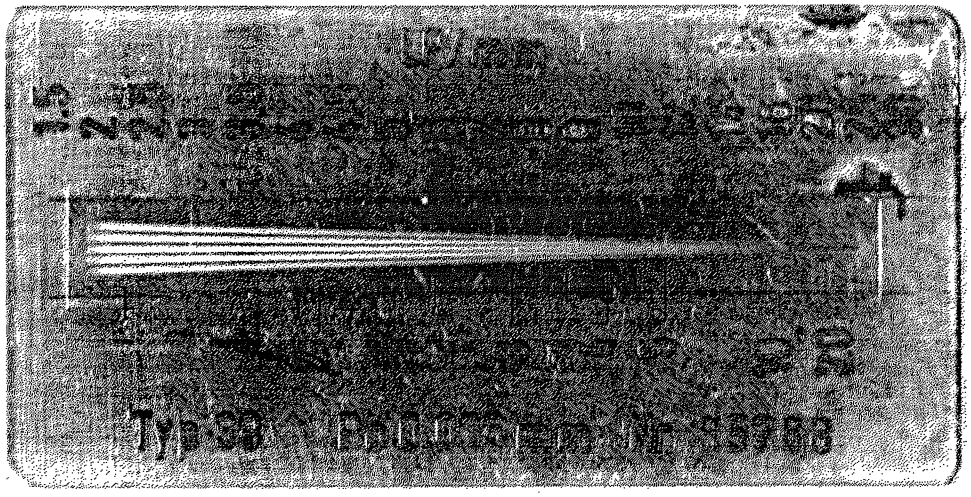

Figure 11: Star-test pattern used (Hüttner Typ 39, Besentest, 25 lp/mm). The pattern is cut in a 25 µm thick layer of lead, fixed between 1 mm thick perspex discs.

4.5 Parameters changed during experiment

4.5.1 Filtering

The energy distribution of electrons in the plasma covers a large energy range, up to the MeV region. It can be assumed that electrons with higher energy penetrate deeper into the surrounding target material than electrons with lower energy. This would result in a larger fraction of high-energy photons further away from the centre of the plasma. Consequently the source should appear larger when observing at higher photon energies, i.e. observing filtered radiation. Measurements with different filters have been done to investigate this effect. Using different materials and different thicknesses of the filters, the recorded intensity originating from different parts of the X-ray energy spectrum was changed according to Figure 18.

4.5.2 Change of laser parameters

It is not obvious how different laser parameters influence the source size, due to the complex interaction processes that occur when X-rays are generated by LPP:s.

Therefore the following laser parameters were changed and the source sizes were measured:

Pulse energy: The main pulse energy can be adjusted up to the maximum energy. All energies measured in the experiments were measured before pulse compression. The energy on the target is approximately half this energy.

Prepulse: Approximately 11 ns before the main pulse a small prepulse appears. Usually this is minimised to 10^{-6} of the main pulse, but to investigate the influence of this prepulse it has been changed up to $2.4 \cdot 10^{-4}$ of the intensity of the main pulse.

Pulses immediately before the main pulse: Before the main pulse usually some small pulses appear. The appearance of these pulses can be affected by adjustment of the laser system. In Figure 12 these pulses are measured with a photodiode in scattered laser light after the compression, for five different settings. The rise time of the diode is <1 ns. The short pulses appear distorted in the figures due to the slow raise time of the diode. The influence of these pulses on the source size have been investigated.

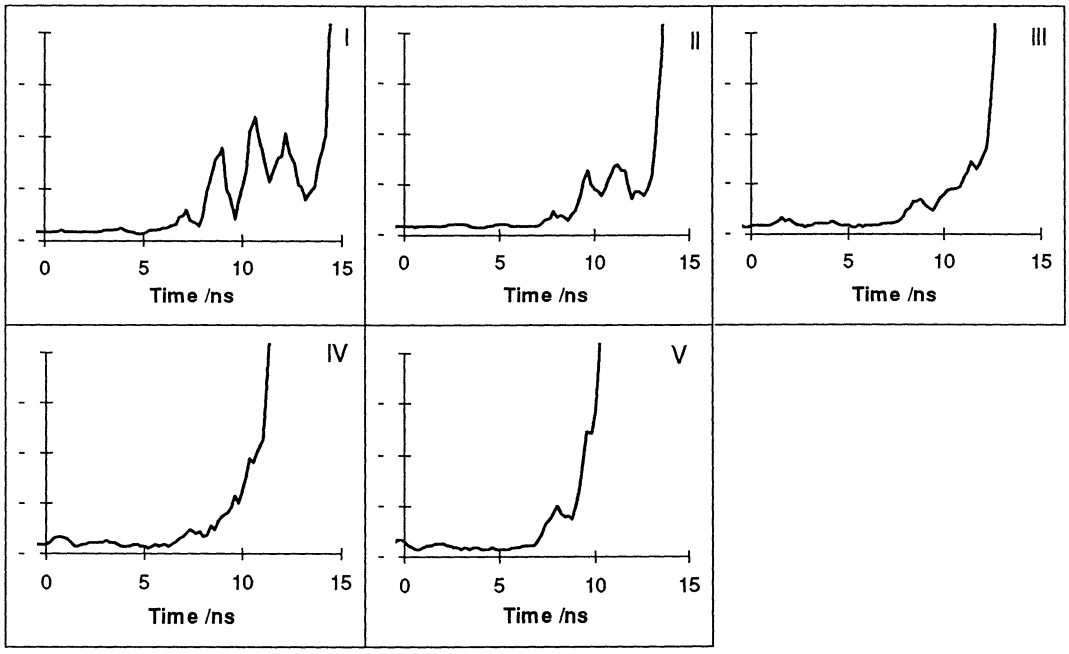

Figure 12: Pulses immediately before the raising edge of the main laser-pulse, measured with a photodiode with raise-time <1 ns and a sampling oscilloscope with a bandwidth of 500 MHz (the pulse-shapes are distorted due to the slow raise-time of the diode in the oscilloscope pictures).

Focal spot size: The size of the laser focal spot was changed by moving the target in and out of focus.

4.6 Evaluation

4.6.1 Measurements with a pinhole camera

The images were recorded with the CCD system and evaluated by taking an averaged intensity profile, 5 pixels wide, at the centre of the pinhole image. A wider averaging

range will give less noise in the intensity profile, but the profile will get affected by the circular shape of the X-ray spot. Since the diameter of the spots were of the order of 30 pixels this effect is small and will be neglected. In all profiles, the full width at half maximum (FWHM) was determined and divided with the magnification to get the FWHM of the source.

The size of the X-ray spot (FWHM) is given by:

$$f = w\frac{a}{b}, \tag{5}$$

where w is the FWHM measured in the picture, a is the source-pinhole distance and b is the pinhole-detector distance. The maximum error in f is then given by:

$$\Delta f = \left|\frac{\partial f}{\partial w}\Delta w\right| + \left|\frac{\partial f}{\partial a}\Delta a\right| + \left|\frac{\partial f}{\partial b}\Delta b\right| = \underbrace{\left|\frac{a}{b}\Delta w\right|}_{\text{read-out error}} + \underbrace{\left|\frac{w}{b}\Delta a\right| + \left|w\frac{a}{b^2}\Delta b\right|}_{\text{error in magnification}}, \tag{6}$$

The read-out error, Δw, was estimated to be 5 pixels, 0.265 mm and 0.11 mm for the two different optical coupling systems, respectively. Δa was estimated to 1 mm and Δb to 10mm. This yields an error of $\Delta f \approx 10$ µm. About 80 % of this error come from the read-out error.

4.6.2 Measurements with a slit

The CCD-system was used for imaging and the pictures were evaluated by taking an intensity profile, averaged over a number of pixels. The FWHM was measured in the intensity profiles. Additionally, a fast Fourier transform (FFT) was applied to the profile to obtain the MTF.

The width of the focal spot is given by the same expression as for the pinhole measurements (eq. 5), and hence the maximum error follows (eq. 6). The read-out error, Δw, was estimated to be 0.15 mm, and the measurement errors in the geometry were estimated to Δa=0.2 cm and Δb=1 cm, respectively.

4.6.3 Measurements with a star-test pattern

Both the image plates and the CCD-system were used for imaging of the star-test pattern. The highest geometrically available magnification was used, to avoid limitations by the resolution of the detectors. The maximum resolution was estimated by visual inspection of the star-test pattern image, after contrast enhancement. The error in determining the limit of resolution was estimated to be ~2 lp/mm. Intensity profiles of the image of the pattern was also taken at several spatial frequencies, to obtain a CTF-curve.

4.6.4 Measurements with a thread

A slit, 20 pixel wide, perpendicular to the thread was used for image evaluation. An average over these 20 pixels was taken and plotted against position (Figure 13). To get a reproducible measure of the distance S (equal to the WRDEAM), the height h was taken. Thereafter the curve was differentiated to easily find the maximum slope k of the curve, and the distance S was calculated as $S=h/k$. After differentiation, a moving average over 5 points was taken. This was found to be convenient to reduce the influence of noise without noticeably affecting the maximum value of the slope.

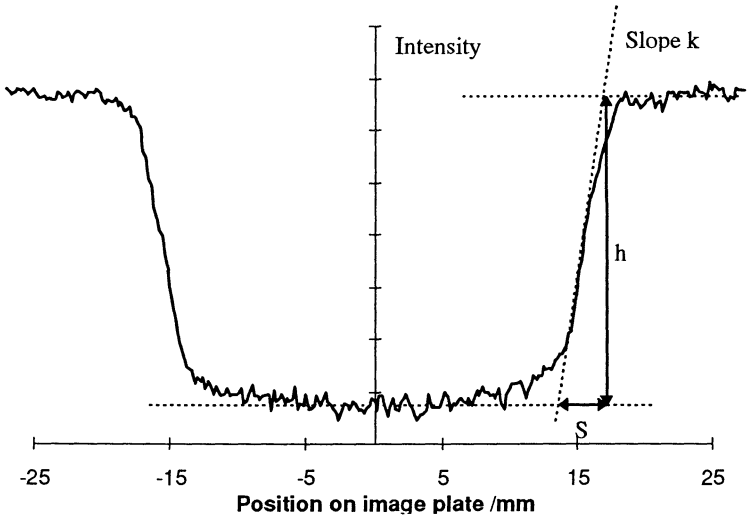

Figure 13: Intensity profile from thread measurement. The width of the blurred zone S corresponds to the WRDEAM of the source.

The size of the source has been calculated as:

$$f = \frac{ha}{kb}, \tag{7}$$

where a is the distance between the target and the object (the thread), b is the distance between the object and the detector, h is the height of the intensity profile, and k is the maximum slope of the intensity profile (se Figure 13). The maximum error was estimated as:

$$\Delta f = \left|\frac{\partial f}{\partial h}\Delta h\right| + \left|\frac{\partial f}{\partial k}\Delta k\right| + \left|\frac{\partial f}{\partial a}\Delta a\right| + \left|\frac{\partial f}{\partial b}\Delta b\right| \tag{8}$$

The error Δa was estimated to 0.5 mm, Δb to 5 mm, Δh to 3 % of h and Δk to 10 % of k. This yields maximum errors of around 10 µm. About 80 % of this error comes from the read-out error.

Correction factors for transmission through the peripheral parts of the thread

The thread's absorption is considered as a step function in the mathematical analysis of the measurement method. Therefore, an error will be introduced due to partial transmission through the peripheral parts of the thread. An estimation of this error was done by calculating the expected intensity profile of a circular thread irradiated with

monoenergetic photons. This was done for different energies in the range from 10 to 200 keV. The obtained profiles were then weighted with the spectrum of the source, the sensitivity of the image plate and the absorption in the filters used.

A circular thread with 0.5 mm diameter was assumed. Attenuation coefficients for platinum were obtained from the database of the National Nuclear Data Centre[34]. The distance between the source and the object was set to 10 mm and the distance between the object and the image plane was set to 200 mm. These distances are of the same order of magnitude as the distances used in the measurements. The intensity at 20 points in the penumbra region was calculated for 20 energies in the range from 10 to 200 keV. The distribution of a source, assumed to be rectangular with a width of 50 µm, was multiplied with the transmission function of the thread (eq. 9), and then integrated over the source co-ordinate, x. This resulted in 20 intensity profiles for different energies. These were weighted by the spectrum of the source, the sensitivity of the image plates and the absorption of actual filters, resulting in expected intensity profiles for each filter used. The profiles were evaluated in the same way as the measured intensity profiles. The width of the calculated profiles were compared with the calculated width of the penumbra region for a rectangular transmission function. The error due to the circular profile of the thread was found to be between 3 and 10 %, depending on the filtration. As expected the error grows with harder filtration, since the energy spectrum is shifted towards higher energies. The correction factors can be seen in Table 1.

Filter	Correction factor
unfiltered	0.97
0.15mm Cu	0.93
0.45mm Cu	0.90
1.5mm Al	0.95
0.1mm Ta	0.92

Table 1: Correction factors for the error introduced by partial transmission of photons in the peripheral parts of the thread.

A derivation of the transmission function (eq. 9) of the thread can be found in the appendix, and the geometry of the experiment can be seen in Figure 14.

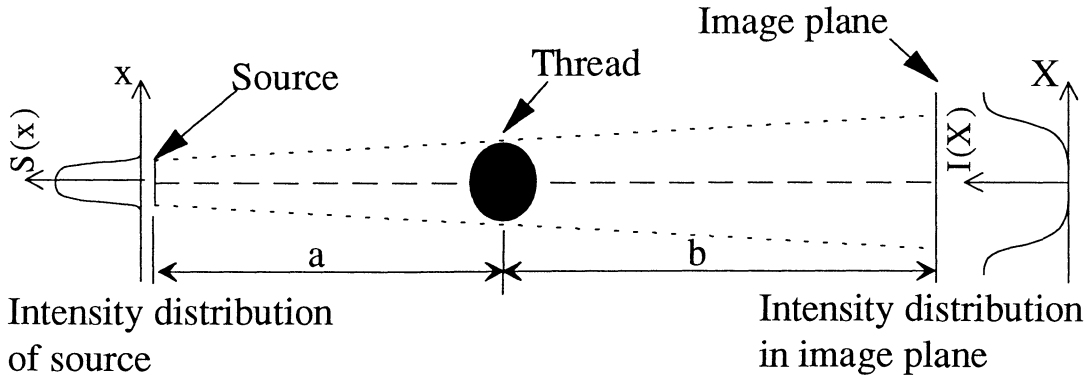

Figure 14: The geometry of the thread measurements.

$$h(x,X)=\begin{cases}\exp\left[-2\sqrt{r^2-a^2\left(\dfrac{X-x}{a+b}+\dfrac{x}{a}\right)^2}\cdot\mu\right] & \text{if transmitted through thread}\\ 1 & \text{otherwise}\end{cases} \quad (9)$$

$$I(X)=\int_{-\infty}^{\infty}S(x)h(x,X)dx \quad (10)$$

This transmission function have been multiplied with an intensity distribution of the source, assumed to be rectangular with a width of 50 μm, and then integrated over the source co-ordinate, x (eq. 10). This way, intensity profiles for monoenergetic radiation from 10 up to 200 keV, in 10 keV intervals, have been calculated. As an example, the profile for 100 keV radiation is found in Figure 15. For comparison the profile obtained for a rectangular transmission function is shown in the same figure.

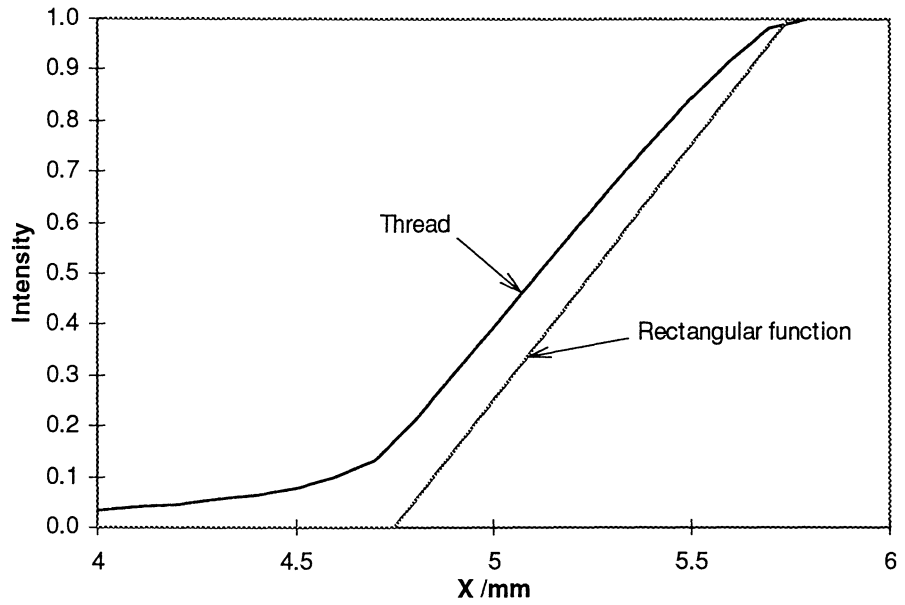

Figure 15: Computed intensity profile in the image plane for 100 keV radiation with a thread as transmission function, to be compared with the intensity profile of a rectangular transmission function with the same width as the diameter of the thread.

To calculate the profile recorded by the image plate, the intensity profiles were weighted by the spectrum of the source, the transmission of the filters and the sensitivity of the image plate. The read out value of the image plates was assumed to be proportional to the energy absorbed by the sensitive layer of the plate. The sensitive layer was assumed to consist of 10% F, 40% Br, 10% I and 40% Ba[37]. The attenuation coefficients for every 10 keV photon energy in the range 10 to 200 keV were downloaded from the National Nuclear Data Centre[34]. The thickness of the layer is 0.15 mm, and the density of the crystal was assumed to be 3.3 g/cm^3 [27]. The attenuation coefficient of the plates can be seen in Figure 16.

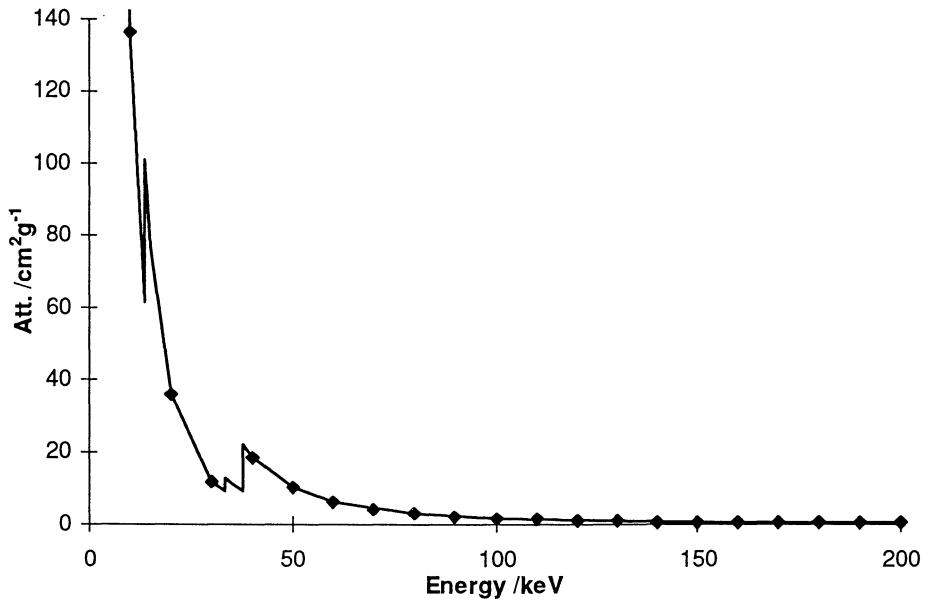

Figure 16: Attenuation coefficient of the sensitive layer of the image plates. Marked points are used for calculations.

The sensitivity of the image plates as a function of energy was calculated according to the formula below:

$$S(E) = E(1 - e^{\mu_{ip}(E)t_{ip}})e^{\mu_f t_f}, \qquad \textbf{(11)}$$

where $S(E)$ is the sensitivity, E is the energy of the photons, μ_{ip} is the attenuation of the sensitive layer of the image plate in cm^{-1}, t_{ip} is the thickness of the sensitive layer, μ_f is the attenuation of the filter and t_f is the thickness of the filter.

By multiplying the sensitivity of the image plate with the fraction of the total number of photons in each energy interval, the contribution of different photon energies to the read-out value of the image plates was calculated. The result for different filtration can be seen in Figure 18. The photon spectrum used for the calculation can be seen in Figure 17.

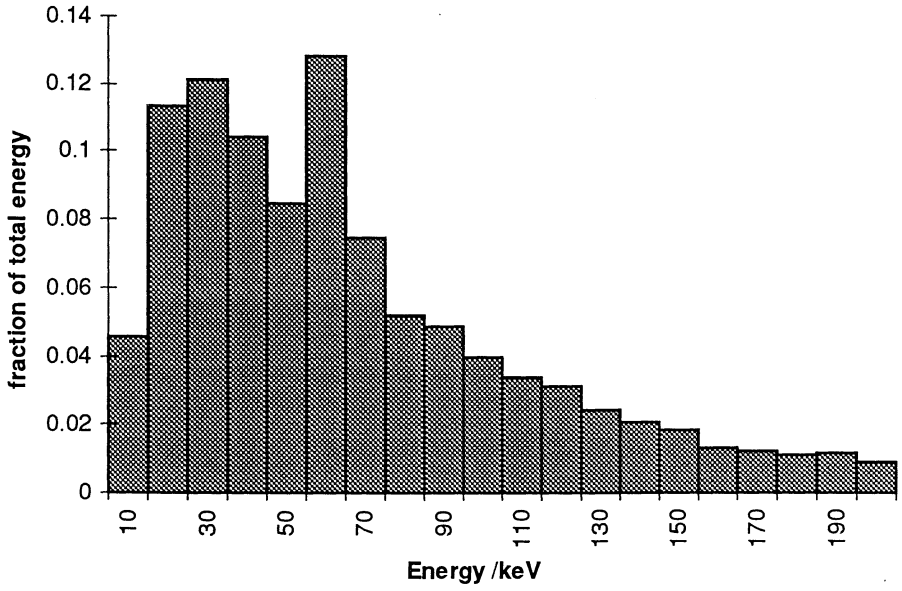

Figure 17: Energy spectrum used for calculations[5].

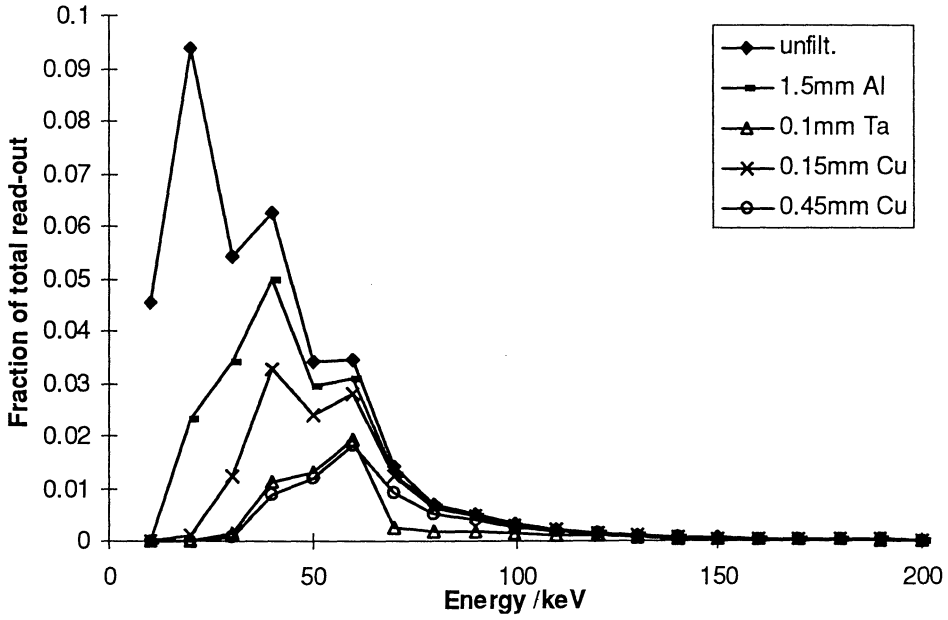

Figure 18: Contribution to the read-out value of the image plates by photons of different energy. The calculations have been done for all filters used.

By weighting the intensity profiles for monoenergetic photons by the spectrum in Figure 18, the expected intensity profile for the actual source was calculated. The profiles were summed according to (eq. 12).

$$I(X) = \sum S(E) I_E(X) = \sum E(1 - e^{\mu_{ip}(E) t_{ip}}) e^{\mu_f t_f} I_E(X), \qquad (12)$$

where I(X) is the intensity at X. $I_E(X)$ is the intensity at X for each energy E. X is the co-ordinate in the image plane (see Figure 14).

The profile for unfiltered radiation can be seen in Figure 19. The profile of a rectangular transmission function with the same width as the diameter of the thread is also plotted in the same graph. As can be seen the height and the maximum slope of the two profiles are not differing very much. The difference in WRDEAM calculated from the two curves is about 3%.

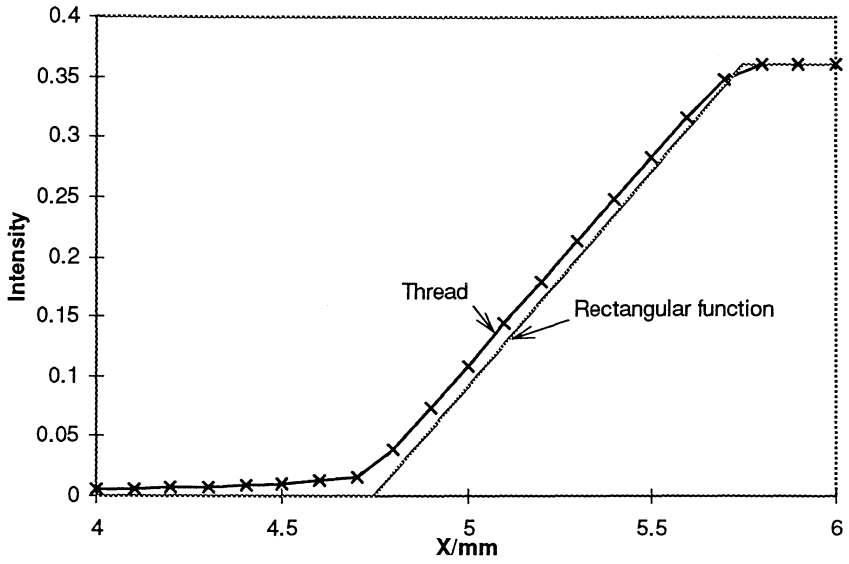

Figure 19: Sum of computed intensity profiles, 10 to 200 keV monoenergetic photons, weighted by the energy spectrum of the source and the sensitivity of the image plates. No filter was used. For comparison, the profile of a rectangular transmission function with the same width as the diameter of the thread is also plotted.

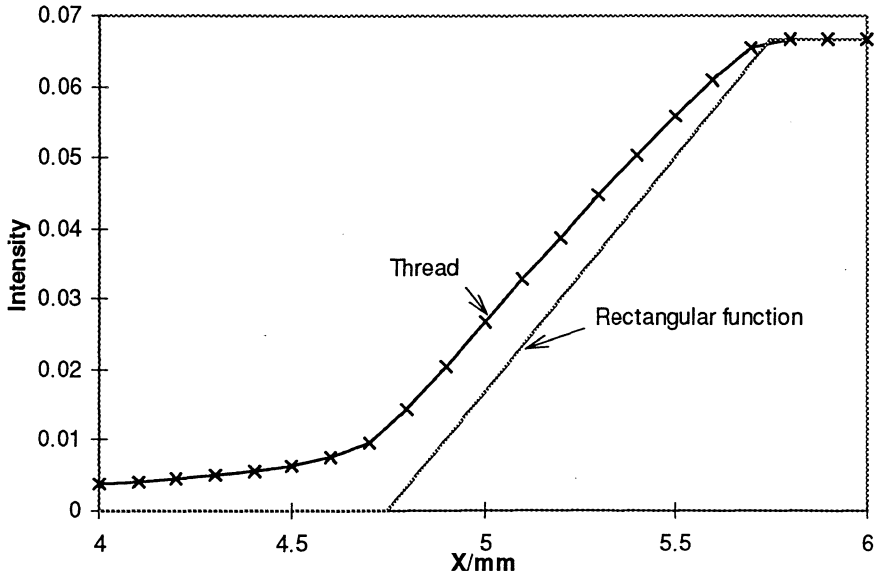

Figure 20: Sum of computed intensity profiles. The same conditions as in Figure 19, but with 0.45 mm Cu filtration.

5. Results

5.1 Measurements with a pinhole camera

Most of the measurements with varying laser parameters have been done with a pinhole camera, since this method showed out to be reliable, and gave two-dimensional information on the intensity distribution of the source.

5.1.1 Measurements with a 5 μm pinhole

In the first series of pinhole measurements only one exposure for each setting was done. The intensity distribution and the FWHM were measured both vertically and horizontally. Very large fluctuations between measurements with similar settings can be seen in the results. This makes it difficult to draw any conclusions from variations in source size upon changes in laser parameters. A laser energy of 300 mJ (measured before pulse compression), exposure times between 120 and 240 seconds, and 3 cm source to object distance and 100 cm object to detector distance, yielding 33 times magnification were used.

The smallest measured source size

The smallest source size recorded was (32±9) μm vertically and (34±9) μm horizontally (FWHM). This shows the potential of the laser-produced plasma as a small source for magnification radiography, as soon as the large fluctuations in size can be overcome. The image of the source shows that the intensity distribution is almost circular (Figure 21).

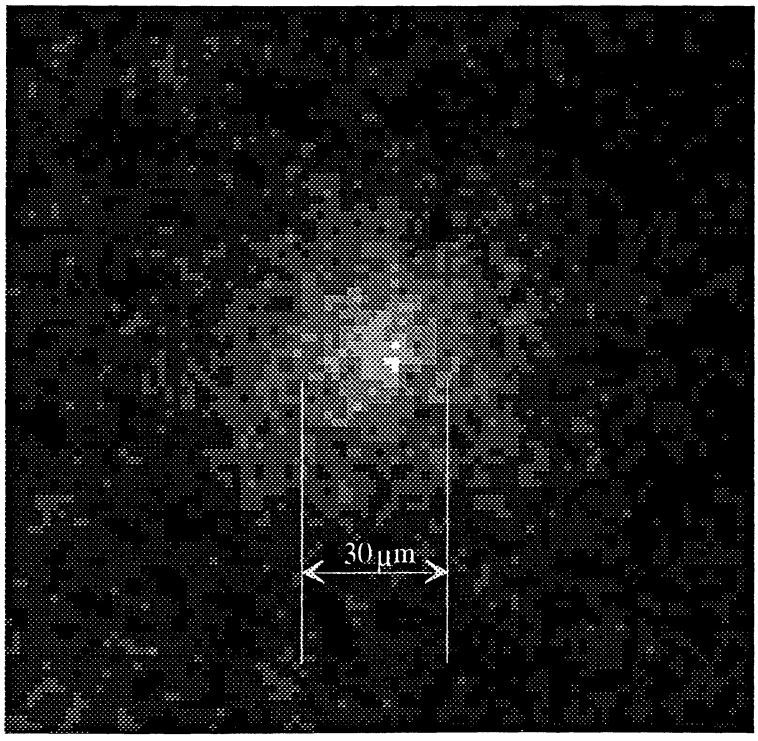

Figure 21: Pinhole image of the source. In the image can be seen that the intensity distribution is almost circular.

Intensity distribution of the source

The measured intensity distribution corresponds well to a Lorentzian curve. In many cases it is easier to do calculations for a Gaussian distribution, and as can be seen in Figure 22 this is a good approximation, too. Filtration of the radiation did not change the distribution noticeably.

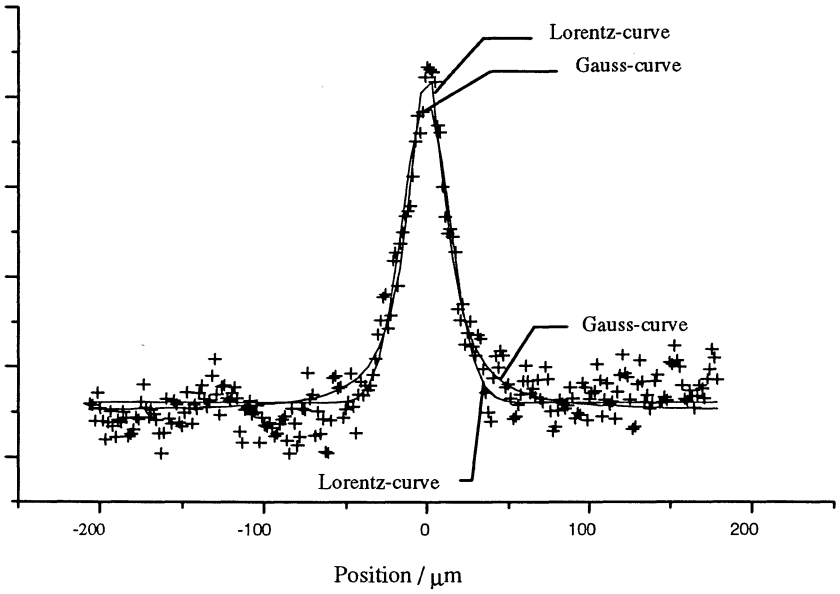

Figure 22: Intensity distribution of source, measured with 5 µm pin-hole.

Source size as a function of the laser spot size at the target

The target was moved in and out of focus, and images were taken at different positions. In Figure 23 the source size is plotted as a function of target position relative to the focus of the parabolic mirror. The source size increases when the target is out of focus, since the laser spot is larger there.

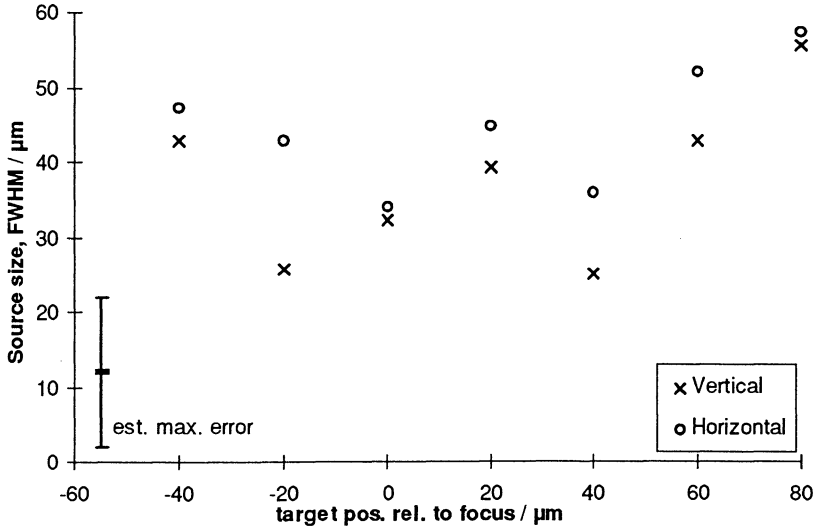

Figure 23: Source size as a function of the target position relative to the focus of the parabolic mirror.

Source size with and without glass plate

By accident a few exposures were done without the glass plate protecting the mirror (see Figure 6). In Figure 24 these exposures are plotted together with the exposures with glass plate, taken immediately before and after. However, it is difficult do draw any conclusions from these measurements, since different mirrors were used in the exposures, possibly affecting the size of the source. An interesting effect is that it seems like the vertical source size is decreasing when the glass plate is removed, but the horizontal source size is remaining the same.

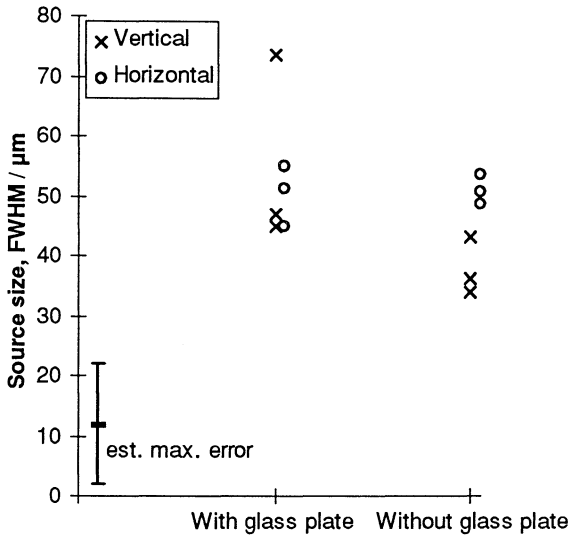

Figure 24: Source size with and without glass plate.

Measurements with different target material

In most of the measurements Ta-targets were used. Some measurements were also done with W-target. No significant change in the source size could be seen. Targets made of copper were tried, but did not give sufficient X-ray yield.

5.1.2 Measurements with a 10 µm pinhole

In the second measurement series the influence of different laser parameters on the source size was investigated. In the measurements, energies above 210 mJ/pulse could not be reached (measured before pulse compression). A 10 µm pinhole was used for this series after the 5 µm hole had clogged up by sputtered particles from the target. The source size had increased much more, compared to the measurements done with the 5 µm hole, than could be expected from the change to a 5 µm larger hole. This could be due to changed pulse duration, giving the plasma time to expand more

Influence of the X-ray energy on the source size

Measurements with filters in different materials and thickness were done in order to investigate how the source size varies depending on the X-ray energy spectrum. In the first measurement series only a few filter measurements were done. The results can be

seen in Figure 25. No significant change in source size could be seen for different filtration. The large spread in the measured sizes at harder filtration could be due to increased noise in these images.

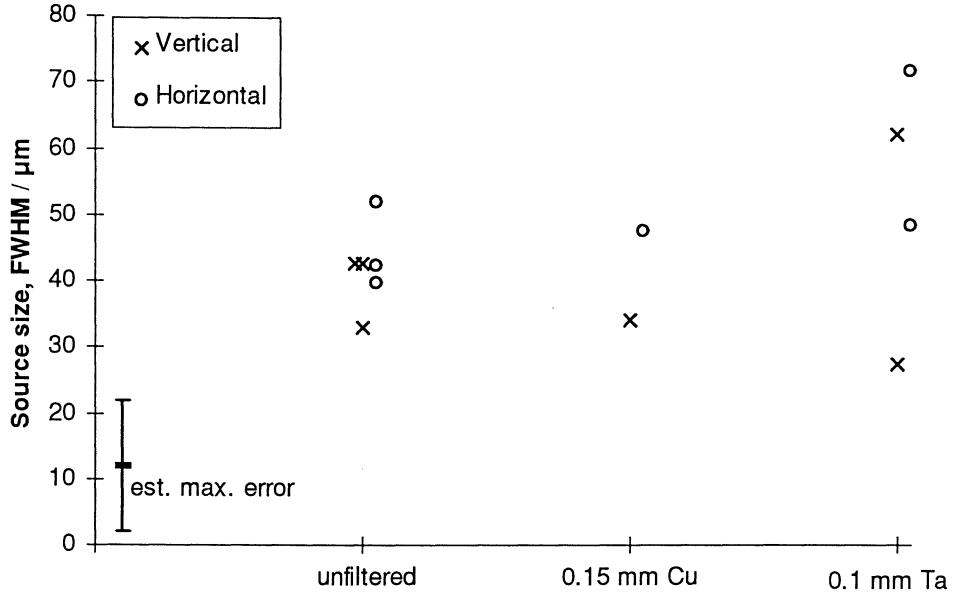

Figure 25: Source size measured with 5 µm pinhole for different filter materials.

In the second measurement series various copper filters were used. The results are presented in Figure 26. Here an increase in source size can be seen when filters are introduced. No significant difference between differently hard filtration was noted.

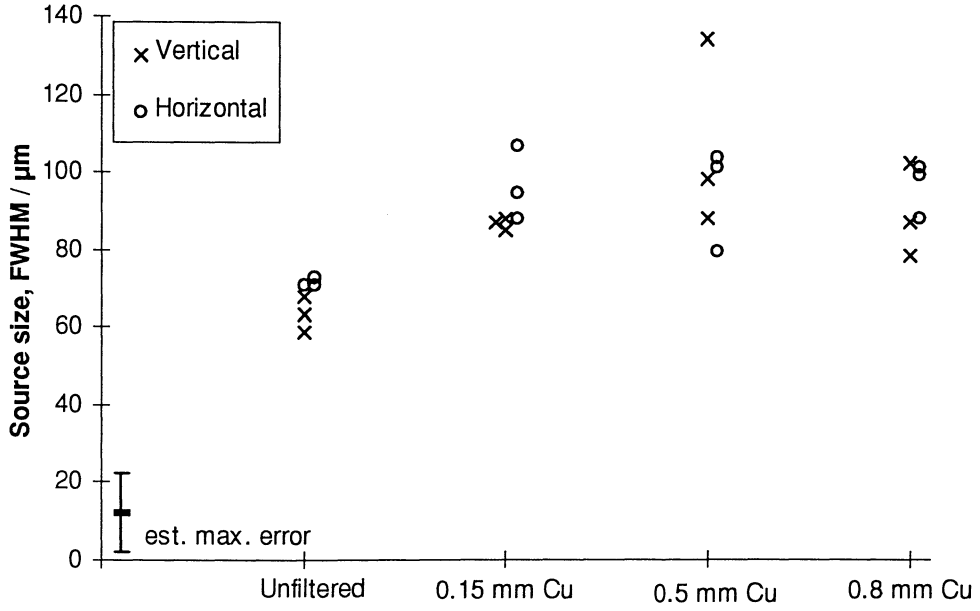

Figure 26: Source size measured with 10 µm pinhole for copper filters of different thickness.

Source size as a function of laser energy

The energy in the laser pulses was changed from 210 mJ down to 65 mJ (20 mJ did not give enough X-rays to give a useable picture). The result is presented in Figure 27. No significant correlation between source size and laser energy could be seen.

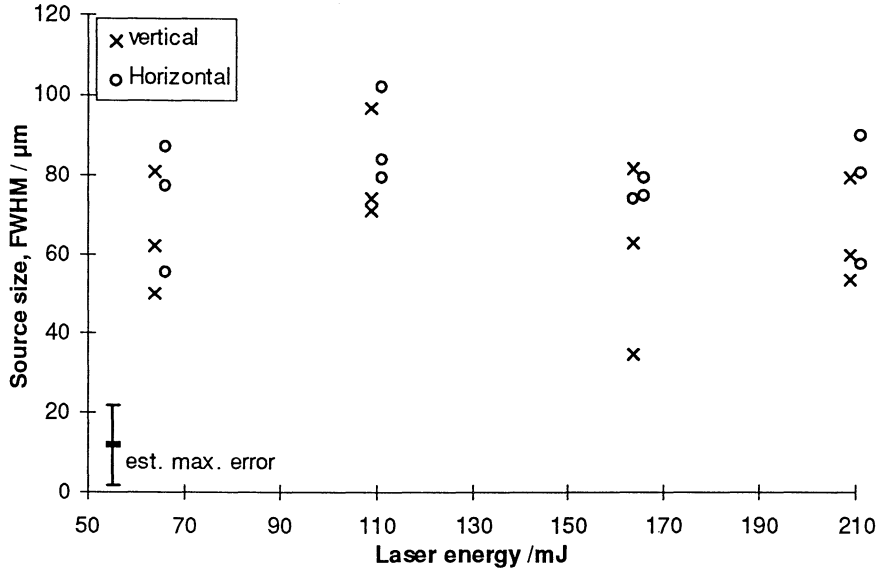

Figure 27 Source size as a function of laser energy

Source size as a function of differently high prepulses

The prepulse, described in 4.5.2, was changed from about 10^{-6} up to $2.4 \cdot 10^{-4}$ times the main pulse. The result can be seen in Figure 28. Here a large spread in the measured source sizes can be seen. This makes it difficult to draw conclusions on the correlation between source size and the intensity of the pre-pulse. However, there does not seem to be any change in the source size.

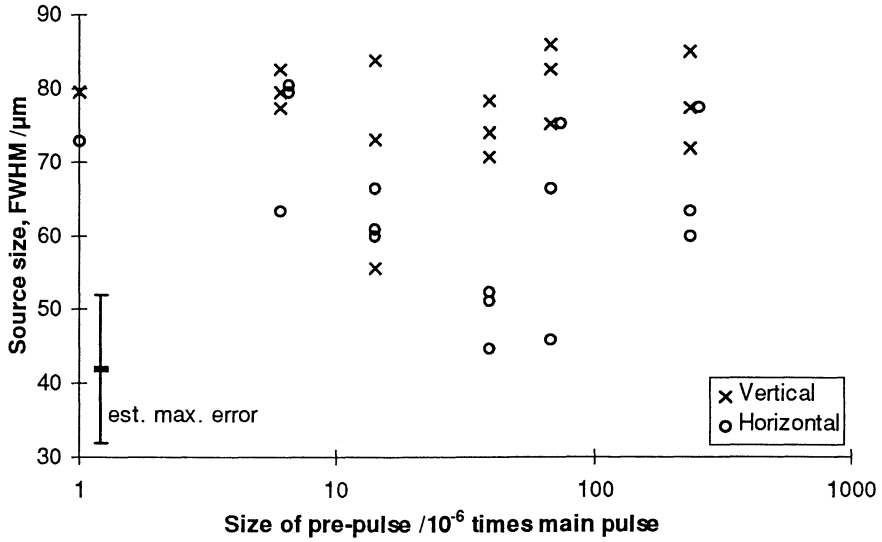

Figure 28: Source size for different laser prepulses.

Influence of pulses before main laser pulse on the size of the source

The appearance of pulses immediately before the main pulse can be changed as described in 4.5.2. The pulses were changed as shown in Figure 12 a-e. The results can be seen in Figure 29. The source size seems to be almost constant during the experiment.

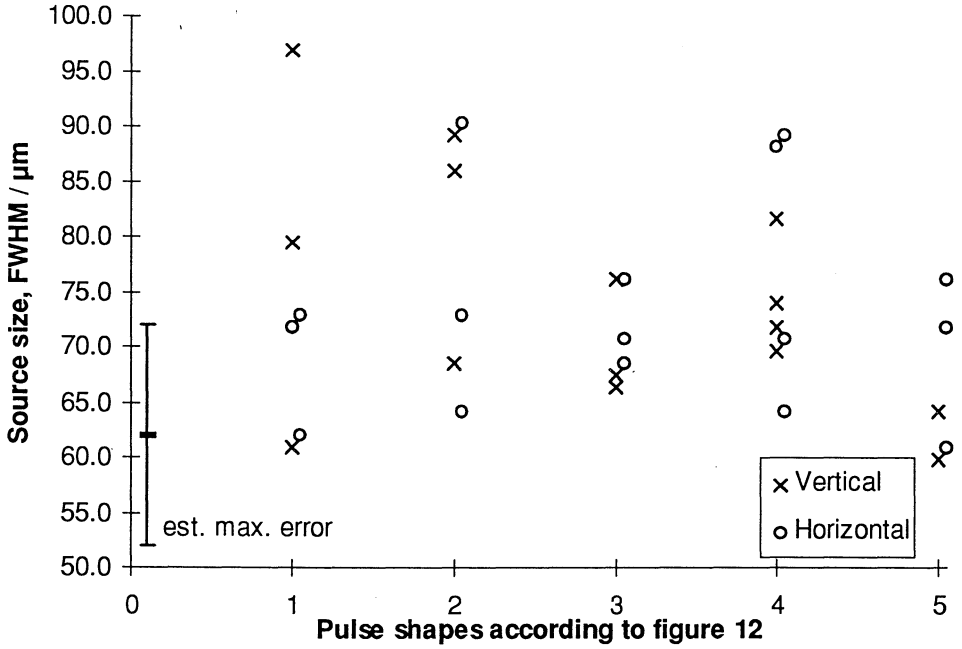

Figure 29: The influence of pulses immediately before the main laser pulse on the source size.

Source size measurement for different surface roughness of the target

Usually the surface of the target is not machined to high surface smoothness. Measurements with a polished tantalum target were tried in comparison to the unpolished target. With a polished target only a few exposures can be done before the surface is covered by sputtered tantalum particles. The X-ray yield of a polished target had shown to be lower than for a rough target surface. The result of the size measurements is presented in Figure 30. Here no significant change in source size can be seen, but the spread in the measured sizes is larger for the polished target. This is unexpected, since the experimental conditions should differ less from shot to shot with this target.

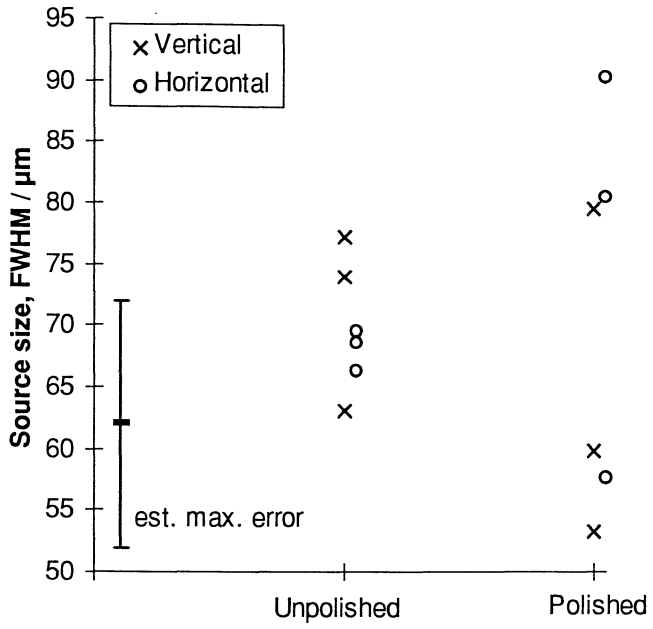

Figure 30: Source size for a polished target compared with a rough target surface.

5.2 Measurements with a slit

The positioning of the slit was not very critical due to the V-shape of the jaws (Figure 8). To make sure that the slit was correctly aligned 5 exposures were done and the slit was moved 0.1 mm perpendicular to the slit direction between each exposure. No significant change in the measured source width was noted. Data for the measurements and the results can be seen in Table 2. All measurements were done with an exposure time of 3 min and with 260 mJ laser energy (measured before pulse compression). The slit was placed at a distance of 8.5 cm from the source and the object to detector distance was 161 cm, yielding a magnification of 19 times. The readout errors were estimated to be ±10 µm. A good estimation of the broadening introduced in the FWHM due to the wide slit used is the width of the slit, 16 µm, resulting in a source size of approximately 40 µm (FWHM).

	Comment	Source size /µm
1	centred	55± 10
2	moved +0.1mm	57±10
3	moved +0.2mm	60±10
4	moved -0.1mm	50±10
5	moved -0.1mm	60±10

Table 2: Measured source sizes with slit (FWHM). Observe that the width of the slit introduces an additive error of approximately 16 µm in all measurements.

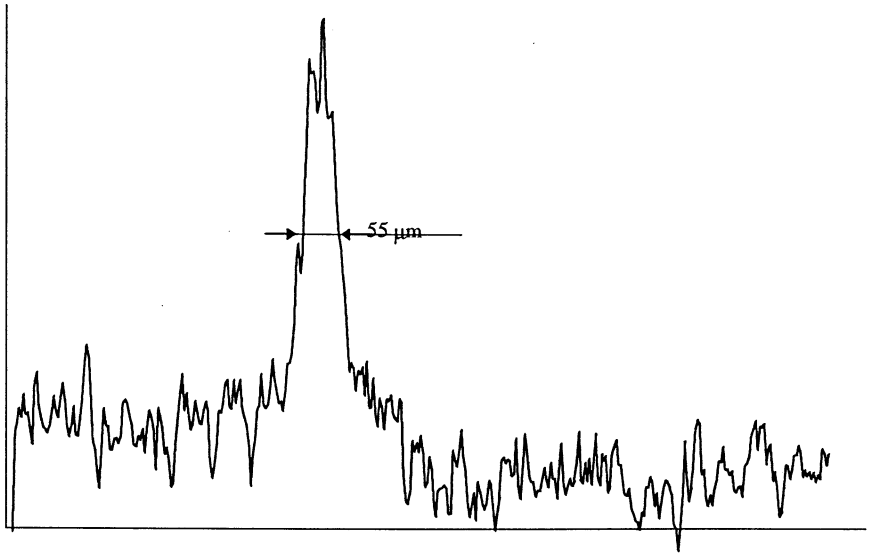

Figure 31: Intensity profile from slit exposure (no 1 in Table 2).

5.2.1 Modulation transfer function analysis

A one-dimensional FFT of the intensity profiles was done to obtain the MTF of the source. The result can be seen in Figure 32. The high value at the lowest frequencies can be assumed to come from low frequency noise in the picture. In Figure 33 the lowest frequencies are removed. By only looking at spatial frequencies above 3 lp/mm the MTF curve gets a more familiar shape (compare with the star-test pattern measurement in Figure 38). The MTF curve goes down to zero at a spatial frequency of approximately 20 lp/mm. This is slightly lower than can be expected from the results of the other measurement methods, but can be explained by the wide slit being used. Instead of a delta function the slit corresponds to a rectangle function, which in the spatial frequency plane corresponds to:

$$f(x)=\begin{cases}1 & if\ -a<x<a \\ 0 & otherwise\end{cases} \quad \overset{FT}{\Longrightarrow} \quad F(\omega)=\frac{2\sin(a\omega)}{\omega} \qquad \textbf{(13)}$$

This is a decaying function in opposite to the Fourier transform of a delta-function, which is constant. The MTF will be modulated with this function, leading to a lower MTF value at higher frequencies.

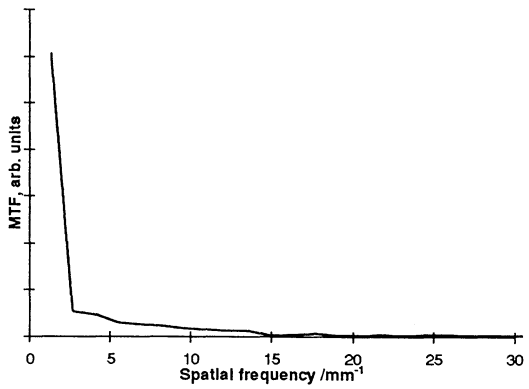

Figure 32: MTF calculated from the slit measurement. The high values at the lowest frequencies are assumed to come from low frequency noise in the picture.

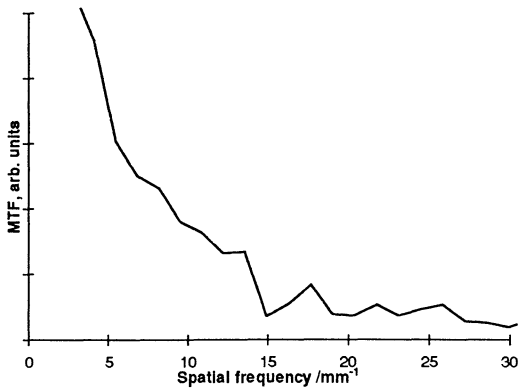

Figure 33: MTF curve calculated from the slit measurement. Frequencies below 3 lp/mm are removed.

5.3 Measurements with a thread

The resulting pictures were evaluated as described in 4.6.4. A typical intensity profile can be seen in Figure 34. The results are presented in Figure 35.

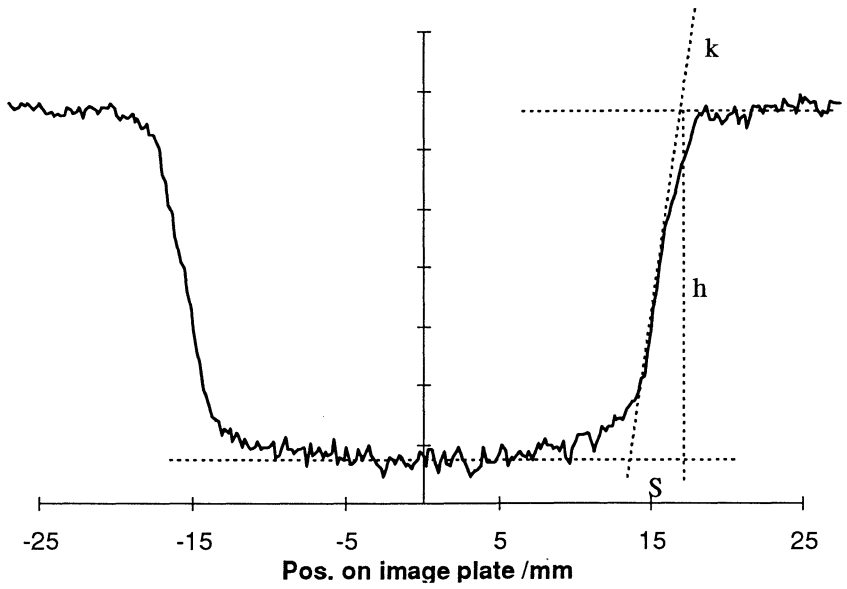

Figure 34: Intensity profile on image plate. 60 times magnification was used. The source-to-object distance was 3.3 cm and the object-to-detector distance was 199 cm. The width of the penumbra region, S, gives the WRDEAM of the source.

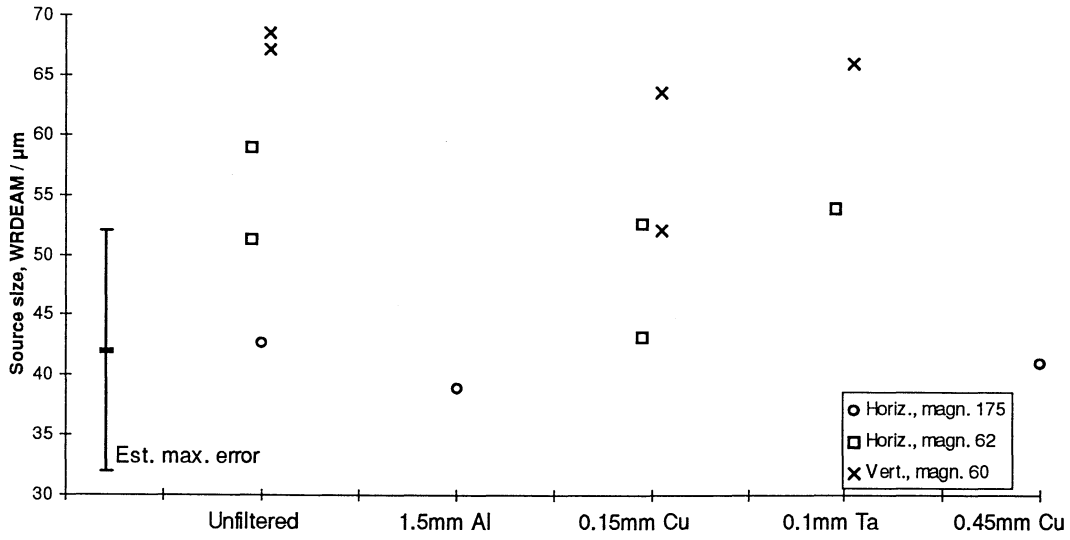

Figure 35: Source size measured with thread and different filtration. The measured sizes are given as WRDEAM. If the source is considered to have a Gaussian intensity distribution the FWHM equals 0.94 WRDEAM.

It should be observed that the stated source widths for all thread measurements are WRDEAM (width of rectangular distribution with equal area and maximum value), while in all other measurements the widths are given as FWHM (full width at half maximum). The relation between these is dependent on the intensity distribution of the source. The pinhole measurement showed that a Gaussian intensity distribution is a good approximation. By assuming a Gaussian intensity distribution, the FWHM is given by:

$$FWHM = 2\sqrt{\frac{\ln 2}{\pi}}\, WRDEAM \approx 0.94\, WRDEAM \qquad \textbf{(14)}$$

The measurements with different filters in Figure 36, have been done in the same exposure for each series, respectively. This gives a good comparison between different filtering. All measurements were done with an exposure time of approximately 5 min and a laser energy of around 270 mJ.

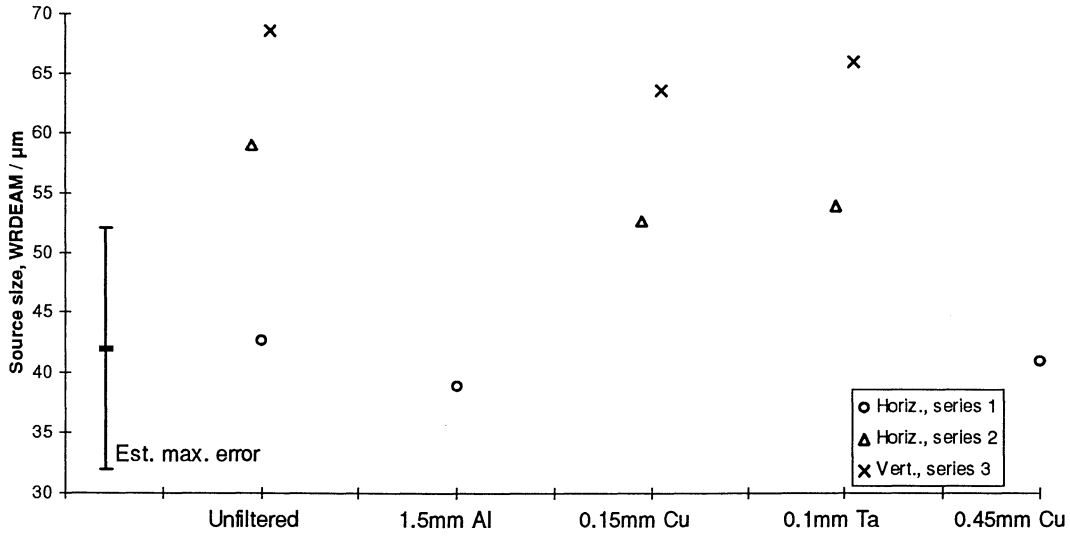

Figure 36: Source size measured with thread and differently thick copper-filters. Three exposures were done. In each exposure a part of the thread was left unfiltered, while the other parts were covered with different filter materials. In this figure each exposure is presented as an own measurement series, guaranteeing that the size of the source was the same within the series.

The smallest source size measured with the thread method was (41±10) µm WRDEAM, horizontally with 1.5 mm Al filtration. This corresponds to (39±10) µm FWHM if the distribution of the source is assumed to be Lorentzian. Simultaneous measurements in both horizontal and vertical directions were not done. Therefore the vertical size in the actual exposure is not known. The smallest vertical size measured with thread was (47±10) µm WRDEAM, with 0.15 mm Cu filtration. This corresponds to (44±10) µm FWHM. The variation of the source size with different filtration is in all cases much less than the measurement errors.

5.4 Resolution measurements with a star-test pattern

The test pattern used was a Hüttner Besentest, 25 lp/mm. The pattern was imaged both on the CCD-system and on image plates. To avoid the limitation of the MTF of the system by the detectors the pattern was magnified, 24 times for the image plates and 19 times for the CCD-system. These were the highest magnifications possible due to geometrical limitations. The pattern could be resolved down to approximately 23 lp/mm both with the image plates (Figure 37) and the CCD-camera. The images were taken with the pattern fixed vertically (hence giving information on the horizontal dimension of the source).

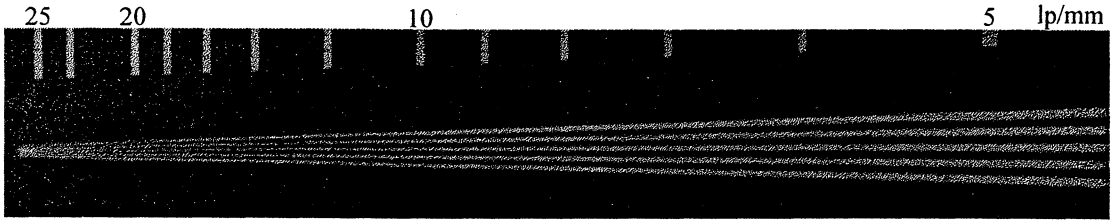

Figure 37: Image of star-test pattern taken with image plate and 24 times magnification. The pattern could be resolved down to approximately 23 lp/mm.

The MTF for a source of effective size, a, is given by (eq. 15), where f_0 is the spatial frequency of a test-object of sinusoidal transmission and m is the magnification used[35].

$$MTF(f_0) = \frac{\sin(\pi f_0 a \frac{m-1}{m})}{\pi f_0 a \frac{m-1}{m}} \qquad (15)$$

The first blurred region in the image of the line pattern corresponds to the first zero of this equation, giving the following expression for the source size as a function of the maximum resolvable spatial frequency:

$$a = \frac{m}{f_0 (m-1)} \qquad (16)$$

Inserting the spatial frequency (23±2) lp/mm and the magnification gives an effective source size of (45±5) μm for the image plate measurements. The CCD-measurements gave a source size of (46±5) μm. These values correspond well to the other measurement methods. It should be observed that this is not the FWHM of the source, but the size of a rectangular intensity distribution with the same maximum MTF. This is a measure of how small the focus of a conventional X-ray tube has to be to give the same resolving power (conventional X-ray tubes have a nearly rectangular intensity distribution).

By taking intensity profiles across the test pattern at different spatial frequencies and calculate the contrast in the profiles, a CTF curve was calculated. The result can be seen in Figure 38.

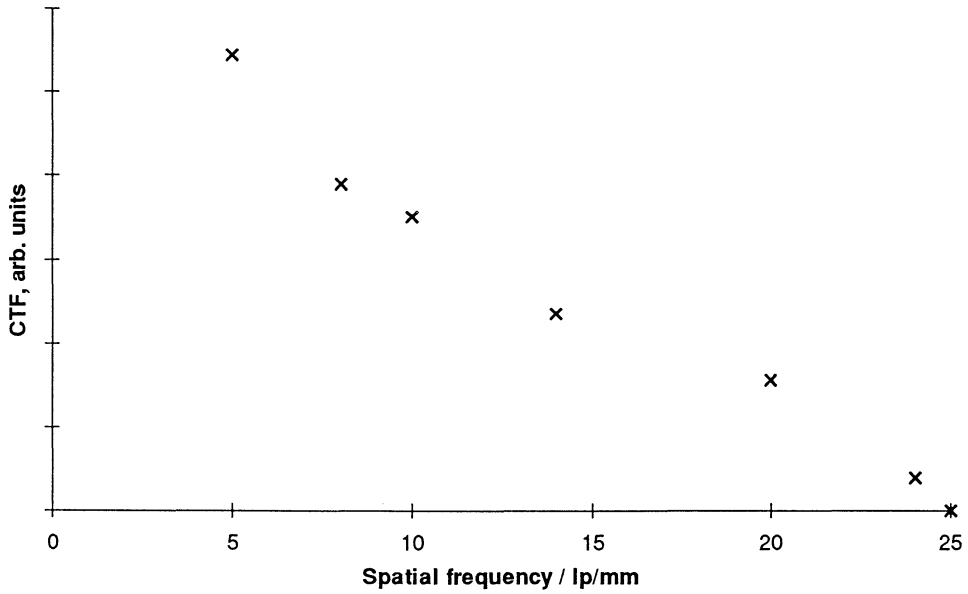

Figure 38: CTF calculated from star-test pattern image.

6. Discussion

6.1 Methods

All measurement methods gave similar results. The errors for all methods except the star-test pattern were of the same order of magnitude. The star-test pattern gave smaller measurement errors, but the method does not give direct information on the source size and distribution. To estimate the source size from the resolution the distribution of the source was assumed to be rectangular. This is a systematic error giving a too large FWHM. This will anyway give an indication of how small the focus of a conventional tube has to be to be equivalent to the LPP, and, most important, the method gives a direct measure of the resolution of the system. Most of the measurements were done with pin-holes. The strength of this method is that it is easy to evaluate and gives two-dimensional information of the intensity distribution. The strength of the thread method is that the size can be measured with different filtration in the same exposure. This was used to examine the source size for different photon energy ranges. The drawback of the method is that the deconvolution is more complicated than for the other methods. Finally, the slit method gives an easy-to-read-out, one-dimensional measure of the intensity distribution with better statistics than the pin-hole method, provided that the slit can be made narrow enough. The slit used in this study was too wide to obtain sufficiently good results.

6.2 Results

The smallest source sizes measured with the pinhole was (32±9) µm vertically and (34±9) µm horizontally (FWHM). This shows the potential of the LPP as an X-ray source for magnification radiography. The range of electrons with a, for laser-produced plasmas, typical energy of 50 keV, calculated by CSDA (continuos slowing down approximation) is 5 µm in tungsten[36]. The size of the X-ray source should therefore be around 10 µm larger than the size of the laser spot on the target. This yields that the diameter of the focal spot of the laser beam is approximately 20 µm, in agreement with previous measurements. It is possible that even smaller focus sizes can be reached by improvements in the focusing optics and the beam transport. The focal spot can theoretically be decreased down to ~3 µm[37]. It would therefore be realistic to expect that a source size in the order of 15 µm is possible with optimal beam transportation and focusing optics. A better focusing of the laser beam would probably also increase the X-ray flux in each shot.

The intensity distribution of the X-ray source was well fitted by a Lorentzian curve. It must be kept in mind that not only the FWHM of an X-ray source, but also the spatial distribution influence the maximum resolution. A Gaussian or Lorentzian distribution gives a higher resolving power than a rectangular distribution with the same FWHM. In most of the measurements the size of the source was slightly larger in the horizontal direction. This may be explained by the angle of incidence of the laser pulses on the target.

It was expected that more soft radiation would come from the centre of the source, and hence the source size should increase slightly with harder filtration. This must be taken into consideration since only harder radiation will penetrate a thicker object and

build up the image. The soft radiation must be filtered away in medical applications since this only gives a contribution to the dose to the patient. Three measurement series were done to investigate the influence of filters, two with pinholes and one with thread. An increased source size could only be seen in one of the pinhole series. In the other measurements, no increase could be seen. Since the thread method should be the most reliable for this kind of measurements, the conclusion from these measurements must be that the filtration does not affect the source size.

The laser energy, the pulses immediately before the main pulse, and the pre-pulse do not seem to influence the source size. If the size of the X-ray source is assumed to be of the same order of size as the laser spot on the target, this is expected. However, these parameters have been shown to influence the X-ray flux[38,39].

The experiment on targets with different surface roughness shows a quite unexpected result. It was known that a rough surface gives a higher X-ray flux, but one would expect that a smother surface would give smaller fluctuations in the source size, since the conditions for each shot are more reproducible. This was not the case. However, only 6 measurements (3 on each target type) were made, and with the large fluctuations in source size in all other measurements in mind, these are too few to draw definite conclusions.

6.3 A comparison of LPP-sources and conventional X-ray tubes

Today there are conventional X-ray tubes with focal spot sizes below 20 μm[20]. This is of the same order of magnitude as the smallest source sizes the laser produced plasmas can be expected to give rise to. The limitation of both the LPP-sources and conventional X-ray tubes with small foci is the low X-ray flux rate, leading to long exposure times. In conventional tubes the heating of the anode and repulsion forces between electrons at higher cathode currents set the limit. In LPP:s the physical constraints limit the flux from each shot. A comparison of the LPP and a conventional microfocus X-ray tube is found in Table 3.

Type of source	**Dose rate (at FOD 75 cm)**
Harwell & Oxford HF200M X-ray tube, at 60 keV, 2.4 mm Al filter (source size <20 μm)	187 μGy/s
Typical value for conventional mammography tube	~30 mGy/s
Laser produced plasma, Ta-target, 0.15 mm Cu filter	1.1 μGy/pulse
Laser produced plasma, Ta-target, 4.5 mm Al filter	0.3 μGy/pulse

Table 3: A comparison of the X-ray flux rate from different X-ray sources.

Different filtrations were used in the measurements with the LPP and the conventional tube. To be able to compare with a HF200M-tube (Harwell & Oxford), the dose rate of the LPP for 2.4 mm Al should be somewhere between the values for 0.15 mm Cu and 4.5 mm Al. This shows that the dose from 200 laser pulses corresponds to one second of irradiation by the X-ray tube. Since the repetition rate of table-top laser

systems today is about 10 Hz the LPP-source is slower than the conventional tube, but systems with higher repetition rates are being developed, with a projected repetition rate of 1000 Hz. This would make it possible to reduce the exposure time. One can also expect a higher dose per pulse by optimisation of the LPP-system with respect to X-ray yield. This has not been done yet. Since the HF200M-tube is already used for magnification radiography of thicker parts of the body, such as joints, and since the LPP-source can be expected to have comparable or better performance it could be an alternative method. The possibility of combining high resolution radiography with time-gated viewing and differential imaging are maybe the most important benefits of the LPP-source.

6.4 Suggested improvements

Since the range of electrons with an energy typical for LPP:s is of the order of 5 µm, one could expect the X-ray source to be approximately 10 µm larger than the focal spot of the laser beam. This focal spot can theoretically be decreased to ~3 µm. Therefore it should be possible to decrease the size of the laser focus by using better focusing optics and laser beam characteristics. A smaller laser focus should lead to a smaller X-ray source and higher X-ray flux. Since the surface roughness of the target influences the X-ray yield[40,41], but not the source size, this should be investigated further. One suggested way of decreasing the source size is to use targets much thinner than the expected size of the source, fixed on a supporting disc made of some low atomic-number material. This should concentrate the electron interactions in the target to the region near the centre of the laser focus, while a large amount of the electrons usually interacting at longer distances form the centre will pass out to the low-Z material behind. Interactions in this supporting material will lead to less hard X-rays than in high-Z material. However, this would decrease the overall X-ray yield. Better laser systems are being developed with higher pulse energies and higher repetition rates. This will of course increase the mean X-ray flux.

By accident, some exposures were done without the protective glass-plate (Figure 24). The influence of this plate has previously been neglected. In these measurements one can see that the size of the X-ray source in the vertical direction is decreasing, while the size in the horizontal direction is constant. This indicates that the glass plate does influence the size of the laser focus. However, only three measurements without glass plate were done, and safe conclusions can not be drawn, but this effect should be further investigated.

7. Acknowledgements

First of all, I would like to thank my supervisor, Matthias Grätz, who has introduced me to the world of research, and has given me a lot of good advice. He has also helped me with the practical experiments, including lifting the 200 kg of lead each time the experimental chamber had to be opened (a good physical exercise).

Special thanks to Carl Tillman for answering many of my questions concerning laser-produced X-rays, and for being an "extra" supervisor.

I would like to thank Professor Sune Svanberg for giving me the opportunity to do this work.

I would also like to thank Gudmund Svahn at the department of diagnostic radiology, Lund University Hospital, for lending me the slit.

Finally, I would like to thank all people involved in my work at the division of atomic physics at the Lund Institute of Technology.

8. Abbreviations

CSDA	continuous slowing down approximation
CCD	charge-coupled device
CTF	contrast transfer function
ESF	edge spread function
FFT	fast Fourier transform
FOD	focus-to-object distance
FT	Fourier transform
FWHM	full width at half maximum
LPP	laser produced plasma
LSF	line spread function
MTF	modulation transfer function
PSF	point spread function
SEM	scanning electron microscope
WRDEAM	width of a rectangular distribution with equal area and maximum value

9. References

[1] W. C. Röntgen: Sitzungsberichten der Physikal.-Medicin. Gesellschaft 132 (Würzburg 1895), English translation in Nature **53**, p 274 (1896)

[2] T. S. Curry, J. E. Dowdey, R. C. Murry: *Christensen's physics of diagnostic radiology*, 4:th ed., Lea & Febiger (1990)

[3] W.-R. Dix: *Intravenous coronary angiography with synchrotron* radiation, Prog. Biophys. molec. Biol. **63**, pp 159-191 (1995)

[4] F. A. Dilmanian, X. Y. Wu, E. C. Parsons, B. Ren, J. Kress, T. M. Button, L. D. Chapman, J. A. Coerre, F. Giron, D. Greenberg, D. J. Krus, Z. Liang, S. Marocovici, M. J. Petersen, C. T. Roque, M. Shleifer, D. N. Slatkin, W. C. Thomlinson, K. Yamamoto, Z. Zhong: *Single- and dual-energy CT with monochromatic synchrotron X-rays*, Phys. Med. Biol. **42**, pp 371-387 (1997)

[5] C. Tillman: *Development and Characterisation of a Laser-Based Hard X-ray Source*, Doctoral Thesis, **LRAP-204**, Lund Institute of Technology, Lund, Sweden (1996)

[6] S. Svanberg, J. Larsson, A. Persson, C-G Wahlström: *Lund High-Power Laser Facility - Systems and first results*, Phys. Scr. **49**, pp 187-197 (1994)

[7] A. Krol, A. Ikhlef, J. C. Kieffer, D. A. Bassano, C. C. Chamberlain: *Laser-based microfocused X-ray source for mammography: Feasibility study*, Submitted to Med. Phys.

[8] K. Herrlin, G. Svahn, C. Ohlsson, H. Pettersson, C. Tillman, A. Persson, C.-G. Wahlström, S. Svanberg: *Generation of X Rays for medical imaging by high-power lasers: Preliminary results*, Radiology **189**, pp 65-68 (1993)

[9] M. Grätz, A. Pifferi, C.-G. Wahlström, S. Svanberg: *Propagation of laser produced short X-ray pulses through scattering media: Application to scatter reduced medical imaging*, in S. Svanberg and C-G. Wahlström (eds.), "X-ray Lasers 1996", Institute of Physics, Bristol (1996), pp 539-541

[10] M. Grätz, A. Pifferi, C.-G. Wahlström, S. Svanberg: *Time-gated imaging in radiology: Theoretical and experimental studies*, accepted for publishing in IEEE Journal of Selected Topics in Quantum Electronics (special issue: Lasers in Medicine and Biology)

[11] B.B. Das, F. Liu and R.R. Alfano: *Time-resolved fluorescence and photon migration studies in biomedical and model random media*, Rep. Prog. Phys. **60**, pp 227-292 (1997)

[12] C. Tillman, I. Mercer, S. Svanberg, K. Herrlin: *Elemental biological imaging by differential absorption using a laser-produced X-ray source*, J. Opt. Soc. Am. B **13** pp 209-215 (1996)

[13] G. U. V. Rao, R. L. Clark, B. W. Gayler: *Radiographic magnification: a critical, theoretical and practical analysis*, part I, Appl. Radiology **1**, pp 37-40+63, part II, Appl. Radiology **2**, pp 25- 33 (1973)

[14] E. T. Kennedy: *Plasmas and Intense Laser Light*, Contemp. Phys. **25:1**, pp 31-58 (1984)

[15] P. K. Carrol, E. T. Kennedy: *Laser-Produced plasmas*, Contemp. Phys **22(1)**, pp 61-96 (1981)

[16] M. D. Perry, G. Mourou: *Terawatt to Petawatt Subpicosecond Lasers*, Science **264**, pp 917-924 (1994)

[17] C. J. Joshi, P. B. Corkum: *Interactions of ultra-intense laser light with matter*, Physics Today **1**, pp 36-43 (1995)
[18] M. Murnane, H. C. Kapteyn, M. D. Rosen, R. W. Falcone: *Ultrafast X-ray pulses from laser-produced plasmas*, Science **251**, pp 531-536 (1991)
[19] J. C. Buckland-Wright, C. R. Bradshaw: *Clinical applications of high-definition microfocal radiography*, Br. J. of Radiology **62**, pp 209-217 (1989)
[20] J. C. Buckland-Wright: *A new high-definition microfocal X-ray unit*, Br. J. of Radiology **62**, pp 201-208 (1989)
[21] E. Hecht: *Optics*, 2:nd ed., Addison-Wesley Publishing Co. (1987)
[22] G. D. Boreman, S. Yang: *Modulation transfer function measurements using three- or four-bar targets*, Appl. Opt. **12**, pp 8050-8052 (1995)
[23] B. Nielsen, G. Fagerberg: *Image quality in mammography with special reference to anti-scatter grids and the magnification technique*, Acta Rad. Diagn. **27**, pp 467-479 (1986)
[24] B. Liu, M. Goodsitt, Heang-Ping Chan: *Normalized average glandular dose in magnification mammography*, Radiology **197**, pp 27-32 (1995)
[25] J. Law: *Patient dose and risk in mammograpy*, Br. J. Radiol. **64**, pp 360-365 (1991)
[26] C. Tillman, G. Grafström, A-C Jonsson, I. Mercer, S. Svanberg, B-A Jönsson, S-E Strand, S. Mattson: *Survival of V79-CH cells studied in vitro after extremely high absorbed dose rate irradiation by X-rays from a laser-produced plasma*, Submitted to Phys. Med. Biol.
[27] J. Miyahara: *The imaging plate: A new radiation image sensor*, Chem. Today **223**, pp 29-36 (1989)
[28] M. Sonada, M. Takano, J. Miyahara, H. Kato: *Computer radiography utilizing scanning laser stimulated luminescence*, Radiology **148**, pp 833-838 (1983)
[29] C. Bueno and M.D. Barker: *High-resolution digital radiography and three-dimensional computed tomography*, Proc. SPIE **2009**, "X-ray Detector Physics and Applications II".(Ed.) V.J. Orphan, pp 179-191 (1993)
[30] J. Dunn, B.K. Young, A.D. Conder, R.E. Stewart: *Detection of 1-100 keV X-rays from high-intensity 500-fs laser-produced plasmas using charge-coupled devices* , Proc. SPIE **2654,** "Solid State Sensor Arrays and CCD Cameras", (Eds.) C.N. Anagnostopoulos, M.M. Blouke, and M.P. Lesser, pp 119-130 (1996)
[31] International Standard, IEC **336**, third ed. (1993)
[32] V. Kaftandjian, Y. M. Zhu, G. Roziere, G. Peix, D. Babot: *A comparison of the Ball, Edge, and Bar/Space pattern techniques for modulation transfer function measurements of linear X-ray detectors*, J. of X-ray Sci. and Tech. **6**, pp 205-221 (1996)
[33] J. U. Maudsen, *Focal spot size measurements for microfocus X-ray sets*, NDT International **22**, pp 292-296 (1989)
[34] National Nuclear Data Center, Brookhaven, "http://www.nndc.bnl.gov/"
[35] R. H. Morgan: *The frequency response function: A valuable means of expressing the informational recording capability of diagnostic X-ray systems*, Am. J. Roentgenol., **88**, pp 175-186 (1962)
[36] F. H. Attix: *Introduction to radiological physics and radiation dosimetry*, John Wiley & Sons (1986)
[37] M. Grätz: *Hard X-rays from a Laser-Produced Plasma: Source Characterization and Applications*, Licenciate Thesis, **LRAP-208**, Lund Institute of Technology, Lund, Sweden (1996)

[38] M. Schnürer, P. V. Nickles, M. P. Kalachnikov, W. Sander, R. Nolte, P. Ambrosi, J. L. Miquel, A. Dulieu, A. Jolas: *Characteristics of hard X-ray emission from subpicosecond laser-produced plasmas*, J. Appl. Phys. **80**, pp 5604-5609 (1996)
[39] J. Steingruber, S. Borgström, T. Starczewski, U. Litzén: *Prepulse dependence of X-ray emission from plasmas created by IR femtosecond laser pulses on solids*, J. Phys. B. **29**, L75-L81 (1996)
[40] S. P. Gordon, T. Donnelly, A. Sullivan, H. Hamster, R. W. Falcone: *X-rays form microstructured targets heated by femtosecond lasers*, Opt. Letters **19:7**, pp 484-486 (1994)
[41] S. P. Gordon, R. Sheppard, T. Donnelly, D. Price, B. White, A. Osterheld, H. Hamster, A. Sullivan, R. W. Falcone: *Short-pulse X-rays form porous targets*, OSA Conf. on "Ultrafast Phenomena", May 2-6 1994, Dana Point, California.

Appendix:

Derivation of the transmission function for a magnified thread:

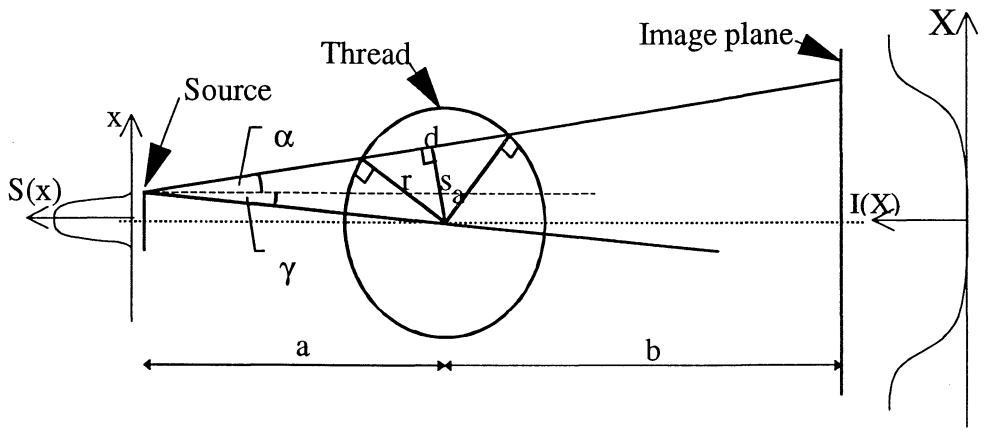

Figure 1: The geometry of the experimental set-up.

The tranmission function for photons is a function of the spatial coordinat of the source and of the image plane, x and X, respectively. The transmission is depending exponentially on the distance the photons have to penetrate the thread, d. d is given by the following expression:

$$d = 2\sqrt{r^2 - s_a^2}, \qquad \text{where}$$

$$s_a = \underbrace{\sqrt{a^2 + x^2}}_{I}\underbrace{\sin(\alpha + \gamma)}_{II}$$

Since the distance a is much smaller than the distance b in all measurements, the following approximations can be done:

I:

$$a >> x \quad \Rightarrow \quad \sqrt{a^2 + x^2} \approx a$$

II:

$$\alpha = \arctan\frac{X - x}{a + b}$$

$$\frac{X - x}{a + b} \text{ is small} \Rightarrow \alpha \approx \frac{X - x}{a + b}$$

$$\gamma = \arctan\frac{x}{a}$$

$$\frac{x}{a} \text{ is small} \Rightarrow \gamma \approx \frac{x}{a}$$

Both α and γ are small $\Rightarrow \sin(\alpha+\gamma) \approx \alpha+\gamma \approx \frac{X-x}{a+b}+\frac{x}{a}$

This gives the following transmission function:

$$h(x,X) = \begin{cases} e^{-d\mu} \approx \exp\left[-2\sqrt{r^2 - a^2\left(\frac{X-x}{a+b}+\frac{x}{a}\right)^2}\cdot\mu\right] & \text{if } d \text{ real} \\ 1 & \text{otherwise} \end{cases},$$

giving the intensity distribution in the image plane, $I(X)$, as

$$I(X) = \int_{-\infty}^{\infty} S(x)h(x,X)dx \quad ,$$

where $S(x)$ is the intensity distribution of the source.